Cellular/Molecular

Nicotinic Receptor Subunit Distribution in Auditory Cortex: Impact of Aging on Receptor Number and Function

Madan Ghimire,[1] Rui Cai,[1] Lynne Ling,[1] Troy A. Hackett,[2] and Donald M. Caspary[1]
[1]Department of Pharmacology, Southern Illinois University School of Medicine, Springfield, Illinois 62702, and [2]Department of Hearing and Speech Sciences, Vanderbilt University Medical Center, Nashville, Tennessee 37232

The presence of novel or degraded communication sounds likely results in activation of basal forebrain cholinergic neurons increasing release of ACh onto presynaptic and postsynaptic nAChRs in primary auditory cortex (A1). nAChR subtypes include high-affinity heteromeric nAChRs commonly composed of α4 and β2 subunits and low-affinity homomeric nAChRs composed of α7 subunits. In young male FBN rats, we detail the following: (1) the distribution/expression of nAChR subunit transcripts in excitatory (VGluT1) and inhibitory (VGAT) neurons across A1 layers; (2) heteromeric nAChR binding across A1 layers; and (3) nAChR excitability in A1 layer (L) 5 cells. In aged rats, we detailed the impact of aging on A1 nAChR subunit expression across layers, heteromeric nAChR receptor binding, and nAChR excitability of A1 L5 cells. A majority of A1 cells coexpressed transcripts for β2 and α4 with or without α7, while dispersed subpopulations expressed β2 and α7 or α7 alone. nAChR subunit transcripts were expressed in young excitatory and inhibitory neurons across L2–L6. Transcript abundance varied across layers, and was highest for β2 and α4. Significant age-related decreases in nAChR subunit transcript expression (message) and receptor binding (protein) were observed in L2-6, most pronounced in infragranular layers. *In vitro* patch-clamp recordings from L5B pyramidal output neurons showed age-related nAChR subunit-selective reductions in postsynaptic responses to ACh. Age-related losses of nAChR subunits likely impact ways in which A1 neurons respond to ACh release. While the elderly require additional resources to disambiguate degraded speech codes, resources mediated by nAChRs may be compromised with aging.

Key words: **ACh aging; auditory cortex; nAChR distribution**

Significance Statement

When attention is required, cholinergic basal forebrain neurons may trigger increased release of ACh onto auditory neurons in primary auditory cortex (A1). Laminar and phenotypic differences in neuronal nAChR expression determine ways in which A1 neurons respond to release of ACh in challenging acoustic environments. This study detailed the distribution and expression of nAChR subunit transcript and protein across A1 layers in young and aged rats. Results showed a differential distribution of nAChR subunits across A1 layers. Age-related decreases in transcript/protein expression were reflected in age-related subunit specific functional loss of nAChR signaling to ACh application in A1 layer 5. Together, these findings could reflect the age-related decline in selective attention observed in the elderly.

Introduction

Important roles for cortical cholinergic systems in attention and cognitive function have been proposed (Sarter et al., 2006; Goard and Dan, 2009; Bauer et al., 2012; Bloem et al., 2014; Hangya et al., 2015; Ballinger et al., 2016; Gil and Metherate, 2019). Detailed maps of projections from subpopulations of cholinergic neurons in the basal forebrain (BF) onto specific cell subtypes across layers of the primary auditory cortex (A1) support the presence of microcircuits whose putative function results from selective cholinergic activation (Do et al., 2016; Kim et al., 2016; Nelson and Mooney, 2016; Gil and Metherate, 2019).

Cholinergic neurons in BF are believed to increase the release of ACh onto auditory neurons in A1 when attention is needed (Sarter et al., 2001, 2006; Schofield and Hurley, 2018). In the A1,

Received Jan. 13, 2020; revised May 11, 2020; accepted May 27, 2020.

Author contributions: M.G., R.C., L.L., T.A.H., and D.M.C. designed research; M.G., R.C., L.L., and T.A.H. performed research; M.G., R.C., L.L., and T.A.H. analyzed data; M.G., R.C., L.L., T.A.H., and D.M.C. wrote the first draft of the paper; M.G., R.C., L.L., T.A.H., and D.M.C. edited the paper; M.G., R.C., L.L., T.A.H., and D.M.C. wrote the paper.

This work was supported by National Institute on Deafness and Other Communication Disorders DC000151 to D.M.C. and DC015388 to T.A.H. We thank the National Institute on Aging for providing FBN rats; Kaitlyn MacDonald and Laura Stanovich for cell plotting; Dr. Brandon Cox for help with the manuscript; and Dr. Kristin Delfino for help with the statistical analysis.

The authors declare no competing financial interests.

Correspondence should be addressed to Donald M. Caspary at dcaspary@siumed.edu.

https://doi.org/10.1523/JNEUROSCI.0093-20.2020

ACh acts on presynaptic and postsynaptic neuronal nAChRs and muscarinic receptors, likely enhancing top-down cognitive representations while suppressing extraneous acoustic information (Kuchibhotla et al., 2017; Sottile et al., 2017a,b; Askew et al., 2019). This forebrain cholinergic system is linked to circuits that are posited to focus attentive resources on "novel" sounds, speech in challenging environments, and speech degraded by aging (Metherate et al., 1992; Everitt and Robbins, 1997; West and Alain, 2000; Sarter et al., 2006; Leaver et al., 2011; Roberts et al., 2013; Gordon-Salant and Cole, 2016). nAChRs mediate prolonged effects, including long-term facilitation of auditory responses (Bakin and Weinberger, 1996; Kilgard and Merzenich, 1998; Froemke et al., 2007). Older individuals direct cortical cognitive and mnemonic resources to help disambiguate speech, where age-related pathology in the auditory periphery and maladaptive changes in central inhibitory function result in a degraded speech code (Bakin and Weinberger, 1996; Kilgard and Merzenich, 1998; Frisina et al., 2001; Froemke et al., 2007; Pichora-Fuller and Schneider, 2017). Cortical cholinergic circuits may be called on to mitigate age-related change in sensory input (Peelle and Wingfield, 2016).

nAChRs are present on many presynaptic inputs and postsynaptic neurons across the layers of A1 (Parent and Descarries, 2008; Metherate, 2011; Schofield and Hurley, 2018; Colangelo et al., 2019). In CNS, nAChRs are comprised of different combinations of the 17 nAChR subunits, which can be divided into: (1) homomeric, α-bungarotoxin (α-Btgx)-sensitive, generally consisting of five α7 subunits; and (2) heteromeric, α-Btgx-insensitive, which are combinations of α2–6 and β2–4 nAChRs subunits that bind nicotine with high affinity (Gotti et al., 2009; Radnikow and Feldmeyer, 2018). Novel heteromeric, α-Bgtx-sensitive subtypes containing both α7 and β2 subunits have also been described in hippocampus and are potentially present in A1 (Wu et al., 2016). The α4β2 nAChR subtype is thought especially important for regulating cognitive function, but α7 nAChRs also may be involved. A series of recent studies, reviewed in Askew et al. (2019), delineate the role of nAChR activation in the microcircuitry of A1. ACh has been shown to evoke strong nAChR-mediated inward currents from voltage-clamped neocortical output layer (L) 5B pyramidal neurons (Goodman et al., 2011). Nicotine has been shown to enhance cognitive function (Terry et al., 1996; Picciotto and Zoli, 2002; Levin et al., 2006; Evans and Drobes, 2009; Sarter et al., 2009), with human and animal behavioral studies showing improved performance on a variety of tasks with administration of nicotine or specific nAChR agonists.

Here we examined the distribution of major nAChR subunit transcripts across A1 layers in young excitatory and inhibitory neurons using multiplexed FISH. We confirm the presence of assembled nAChRs using receptor binding and electrophysiology in A1 slices. Finally, we use single-chromogenic ISH to show a significant decline in nAChR subunit transcript abundance in A1 layers with aging, consistent with the observed age-related decrease in receptor binding and a functional loss of heteromeric nicotinic cholinergic excitability in L5 pyramidal neurons.

Materials and Methods

Animals. All experiments were conducted using young (4-6 months) and aged (28-33 months) Fischer Brown Norway (FBN) male rats supplied by the National Institute on Aging rodent resource colony where rats were bred and raised at the Charles River Laboratory. *ChAT-Cre* young adult Long-Evans rats [4 months, *LE-Tg(Chat-Cre)5.1Deis*] were purchased from the Rat Resource and Research Center (University of Missouri) and used for chemogenetic tracing and cell labeling. Procedures were performed in accordance with protocols approved by the Laboratory Animal Care and Use Committee of Southern Illinois University School of Medicine.

ISH. As detailed in prior studies (Hackett et al., 2016; Sottile et al., 2017b; Hackett, 2018; Balaram et al., 2019), single-chromogenic ISH and multiplexed FISH were used to detect β2, α4, and α7 transcripts in fresh frozen tissue sections (14 μm) from A1 (Fig. 1). ISH was used for estimation of age-related changes in transcript abundance. FISH was used to determine the laminar distributions of β2, α4, and α7 in two ways: (1) expression by inhibitory and excitatory neurons; and (2) coexpression of β2, α4, and α7 in the same cells. Assays used RNAscope riboprobes, reagents, and protocols produced by Advanced Cell Diagnostics. Briefly, sections were postfixed for 15 min in 4% PFA, incubated in Protease IV for 30 min at 40°C, and in riboprobes for 2 h at 40°C for each target (up to four probes per assay), followed by sequential amplification steps culminating in binding of chromogenic (fast red) or fluorescent conjugates (Alexa-488, Atto-555, Alexa-647, and Alexa-750). ISH- and FISH-reacted sections were counterstained to facilitate identification of brain areas, subdivisions, and cortical areas (ISH: 50% hematoxylin in dH_20, 30 s; FISH: DAPI, 45 s). Multiple controls were used to evaluate target probe specificity (Table 1): (1) The housekeeping gene, *Gapdh*, was used as a positive control for single ISH assays; (2) a multiplex positive control containing three highly characterized housekeeping genes (*Ubc*, ubiquitin C; *Polr2a*, DNA-directed RNA polymerase II subunit RPB1; *Ppib*, cyclophilin B) in channels 1–3, respectively; (3) a negative control probe (*DapB*, dihydrodipicolinate reductase), which is a gene from a soil bacterium (bacillus subtilis strain SMY) that has never yielded specific signal in any tissue samples; and (4) fluorescence amplification steps in the absence of positive control or target probes. These controls revealed that all probes were highly specific with no cross-reactivity between probes or color channels (Fig. 2).

Histochemistry and immunofluorescence. Multifluorescence IHC (IF) was performed in coronal sections containing auditory cortex (Table 2). Sections were rinsed for 30 min in 0.1 M PBS, followed by permeabilization with 0.2% Tween 20 for 1 h and incubation in blocking solution for 2 h (0.1% Tween 20, 2% BSA, 5% donkey serum in 0.1 M PBS). Sections were incubated for 48 h in the primary antibody solution (ChAT 1:100 and NeuN 1:500 in blocking solution; Table 2) at 4°C, rinsed, and then incubated for 2 h in the secondary antibody solution (1:500, Alexa-647 donkey anti-goat, Alexa-750 donkey anti-mouse in blocking solution; Table 2) at room temperature. Control sections were incubated in blocking solution without primary antibodies. All incubations and rinsing steps were performed on a laboratory shaker with constant agitation. AChE histochemistry was performed on an alternate series of sections after Geneser-Jensen and Blackstad (1971). Exemplar sections stained for ChAT/NeuN and AChE were imaged to illustrate the laminar patterns typical of each marker in A1, comparable with those reported previously (Lysakowski et al., 1989).

Imaging. Sections were scanned at high resolution in the Digital Histology Shared Resource at Vanderbilt University Medical Center. Bright field imaging of ISH-reacted sections was conducted at 40× on an SCN400 slide scanner (Leica Microsystems), then imported into National Institutes of Health ImageJ (Fiji) software for analyses of transcript abundance (Schindelin et al., 2012). Slides reacted for FISH were scanned on an Aperio Versa 200 microscope (Leica Microsystems); then each color channel analyzed by cortical layer with a HALO software module designed for quantification of multichannel mRNA (Indica Labs). High-magnification image stacks of FISH-reacted sections (100× objective) and ChAT/NeuN FIHC (40× objective) were obtained with a Nikon 90i epifluorescence microscope and Hamamatsu Orca 4.0 CCD camera, controlled by Nikon Elements AR software. AChE was imaged in bright field in a single plane (20× objective). Maximum intensity projections of deconvolved *z*-plane image stacks were assembled into figures using Adobe Illustrator CS6 (Adobe Systems).

ISH and FISH assays. Quantification of age-related changes in transcript expression (ISH) and phenotyping of nAChR-containing cell types in young-adult tissue (FISH) were derived from three sets of assays

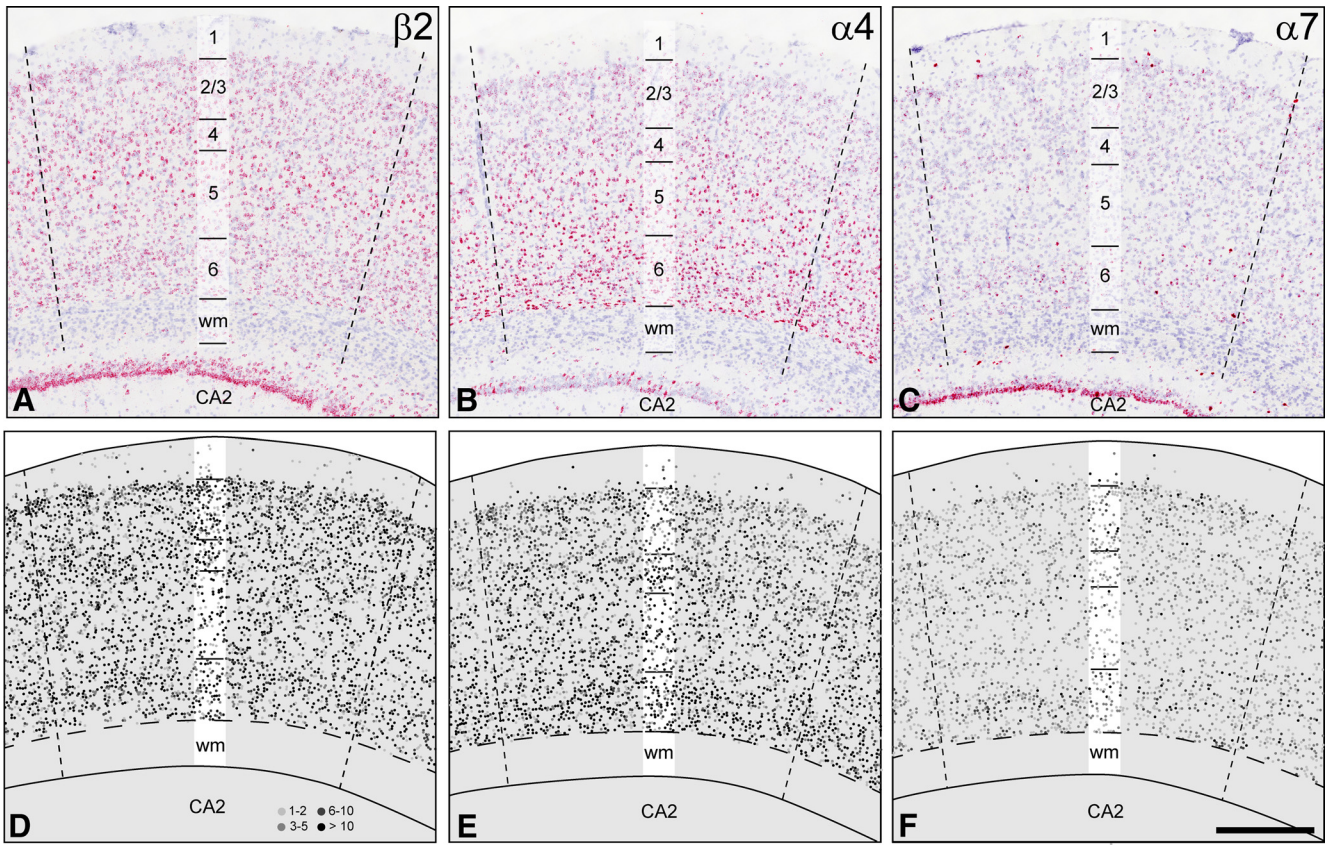

Figure 1. nAChR subunit transcript expression in auditory cortex area A1. ***A–C***, Low power images of β2, α4, and α7 transcript expression (red dots). Blue represents hematoxylin counterstain. ***D–F***, Plots of cells (circular symbols) containing transcripts of each subunit. Symbol shading represents transcript density (1–2, 3–5, 6–10, >10 transcripts/cell). Laminar boundaries indicated in transparent vertical bars. wm, White matter; CA2, cornu ammonis region 2 of hippocampus. Scale bar, 250 μm.

Table 1. Details of rat riboprobes for nAChRs, neuronal class, and controls

Cell type	Protein	Gene	Accession no.	Position
All	Nicotinic receptor subunit, β2	*Chrnb2*	NM_019297.1	197–1668
All	Nicotinic receptor subunit, β4	*Chrnb4*	NM_052806.2	2–1236
All	Nicotinic receptor subunit, α4	*Chrna4*	NM_024354.1	1001–1878
All	Nicotinic receptor subunit, α7	*Chrna7*	NM_012832.3	47–1027
Glutamatergic neurons	Vesicular glutamate transporter 1	*Slc17a7 (VGluT1)*	NM_053859.2	529–1630
Glutamatergic neurons	Vesicular glutamate transporter 2	*Slc17a6 (VGluT2)*	NM_053427.1	1109–2024
GABAergic neurons	Vesicular GABA/glycine transporter	*Slc32a1 (VGAT)*	NM_031782.1	288–1666
Positive control	GAPDH	*Gapdh*	NM_008084.2	21–935
Positive control		*PPIB*	NM_019639.4	34–860
Positive control		*UBC*	NM_009089.2	2802–3678
Positive control		*Polr2a*	NM_011149.2	98-856
Negative control		*dapB*	EF191515	414-862

performed on sequential sections from each brain ($N = 4$ brains per condition).

Set 1 (ISH) assays involved single-probe chromogenic ISH for each nAChR subunit (β2, α4, α7). These assays were used for quantitative measurements of transcript density by layer in young and aged animals. These data also served as a reference of transcript distribution for comparison against multiplex FISH assays using the same riboprobes in young-adult A1. To illustrate laminar distributions, plots of cells containing each nAChR subunit were performed manually from high-resolution images of representative tissue sections, using a pseudo-quantitative scale (Grabinski et al., 2015) (Fig. 1). Cells containing transcripts were denoted by circular symbols with a grayscale fill, scaled by the number of transcripts expressed (1–2, 3–5, 6–10, >10). The X–Y locations of each cell were plotted on schematic diagrams of each subunit and brain region. Quantification of age-related differences in transcript abundance by layer was derived from ISH-reacted sections from the brains of young ($N = 4$) and aged ($N = 4$) animals, as detailed below.

Set 2 assays (nAChR coexpression) combined probes for the β2, α4, and α7 subunits in multiplex FISH assays using young-adult A1 tissue only. The goal was to identify and map the distributions of cellular phenotypes based on subunit coexpression patterns. The number of neurons that coexpressed the principal subunit combinations (e.g., $\alpha4^+\beta2^+\alpha7^-$, $\alpha4^+\beta2^+\alpha7^+$, $\alpha4^-\beta2^-\alpha7^+$) was tallied from both hemispheres of four young-adult brains. Representative plots were generated to show the spatial distribution of each cell type, and charts were created from the cell counts.

Set 3 assays (nAChR expression by neuronal class) combined riboprobes for a single nAChR subunit (β2, α4, or α7) with markers of glutamatergic and GABAergic neurons in multiplex FISH assays using young-adult A1 tissue only. The objective was to quantify and map the

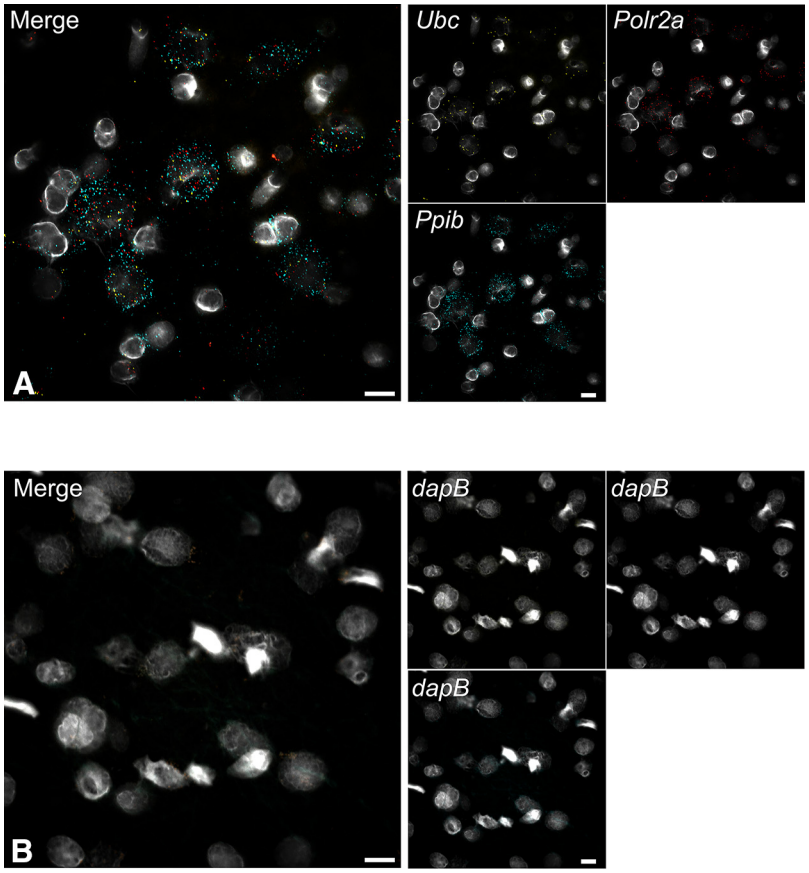

Figure 2. Transcript coexpression controls, FISH assays. ***A***, Positive controls: UBC (yellow dots), Polr2a (red dots), Ppib (aqua dots). ***B***, Negative control: dapB (all color channels). Light gray represents DAPI. Scale bars, 10 µm.

Table 2. Primary and secondary antibodies for chemoarchitecture

Antibody	Species	Supplier	Part #	Dilution
ChAT	Goat	Millipore	AB144P	1:100
NeuN	Mouse	Millipore	MAB377	1:500
Alexa-647 IgG	Donkey anti-goat	Invitrogen	A32930	1:500
Alexa-750 IgG	Donkey anti-mouse	Invitrogen	A32789	1:500

distributions of nAChR subunits expressed by these major neuronal classes. Glutamatergic neurons in cortex were distinguished by expression of vesicular glutamate transporter 1 (*VGluT1*) (Kaneko et al., 2002; Fremeau et al., 2004; Zeisel et al., 2015), which is preferentially expressed by perhaps all glutamatergic cortical neurons. A riboprobe for *VGluT2* was also included in the FISH assay; but since this gene is coexpressed at low levels in subpopulations of cortical *VGluT1*$^+$ neurons, it is not useful for identification of glutamatergic neurons in cortex; rather, *VGluT2* is a principal marker of excitatory neurons in subcortical areas, analyzed for related studies of tissue sections from the same brains (De Gois et al., 2005; Graziano et al., 2008; Ito et al., 2011; Hackett et al., 2016). Inhibitory neurons were identified by expression of the vesicular GABA/glycine transporter (*VGAT*), expressed by GABAergic and glycinergic neurons (Chaudhry et al., 1998; Dumoulin et al., 1999; Zeisel et al., 2015). In cortex, *VGAT* expression is restricted to GABAergic neurons. For each target brain region, the number of glutamatergic and GABAergic neurons that coexpressed each receptor subunit was tallied from both hemispheres of four young-adult brains. Representative plots were generated to show the spatial distribution of each cell type, and charts were created from the cell counts.

Quantification of nAChR expression in young and aged animals. Chromogenic ISH was used for quantitative analysis of potential age-related changes in transcript expression by cortical layer. Autofluorescence artifacts associated with lipofuscin accumulation prohibited reliable analysis of transcript density in aged brain tissue using multiplex FISH that stains with more than one fluorescent marker. Transcript abundance was quantified for each subunit in tissue sections from the brains of 4 young (4–6 months, $N = 4$) and 4 aged (28–33 months) male FBN rats, prepared for Set 1 chromogenic ISH assays (Table 1). Analyses were conducted for each ROI (i.e., subcortical nucleus, cortical layer), after the approach outlined by Grabinski et al. (2015). Slides were scanned as a group at 40× on an SCN400 automated system (Leica Microsystems). The Leica .scn files were imported into ImageJ (Fiji) using the Bio-Formats Importer and converted to RGB.tif files (Fig. 3*A*,*B*). In ISH assays using the fast-red detection kit, single transcripts appear as a single red dot, of ~1 µm diameter (Player et al., 2001; Itzkovitz and van Oudenaarden, 2011; Wang et al., 2012). Image resolution was set at 1 µm/pixel for subsequent analyses. The red signal was separated from the "color threshold" function and YUV indexing (Y = 0, 85–125; U = 0, 255; V = 0, 160–185) (Fig. 3$A_{1'',2''}$, $B_{1'',2''}$). Thresholded images were converted to binary, and particles (transcripts) segregated using the "watershed" function (Fig. 3$A_{1''',2'''}$,$B_{1''',2'''}$). Transcript counts were obtained using the "analyze particles" function. Transcript density in each cortical layer was estimated in two ways: (1) by dividing the particle count for each ROI (i.e., cortical layer) by its area (µm^2); and (2) by dividing the total area occupied by red signal by the area of each layer (µm^2). The latter was judged to produce the most reliable estimate of abundance, as it better accounted for the tightly clustered particles in cells with high transcript density that were not segregated by threshold or watershed functions. For each case, measurements were obtained bilaterally from two tissue sections spaced 126 µm apart. Counts from the four hemispheres were averaged and treated as a single density estimate for each case. This within-subject averaging was done to reduce measurement error due to random variability in staining between tissue sections. Hemispheric differences in expression were not an objective of this study. Transcript density from 4 young and 4 aged animals was compared using a two-tailed paired *t* test for each nAChR subunit and ROI, with statistical significance set at $p < 0.05$.

Quantification of cell number in young and aged animals. DAPI$^+$ cells were counted in A1 of four young and four aged brains using HALO software. Counts of all DAPI-labeled cells were obtained within a 250-µm-wide rectangular bounding box, covering L1–L6. Average cell densities (cells/mm^2) were 1975.7 (SD 20.2) and 1880.6 (SD 101.1) for young and aged brains, respectively. The difference was not significant ($p = 0.16$).

Identification and quantification of cellular phenotypes. For phenotyping (Sets 2 and 3) cell counts for selected combinations of nAChR subunits and cell-type markers were conducted in sections from four young adult brains using a HALO software module designed for analyses of FISH (Indica Labs). As for ISH, transcripts in FISH-reacted tissues appear as a single dot, ~1 µm diameter, in distinct color channels, each corresponding to a single mRNA target. Cells were considered positive for a nAChR subunit or cell type marker if three or more transcripts were located within 5 µm of DAPI-labeled cell nucleus. Cells containing 0–2 transcripts were considered negative. Cells that coexpressed selected combinations of nAChR subunits and cell type markers were used to quantify the density of specific cellular phenotypes by location (cortical layer). For each case, cell counts were obtained bilaterally from two

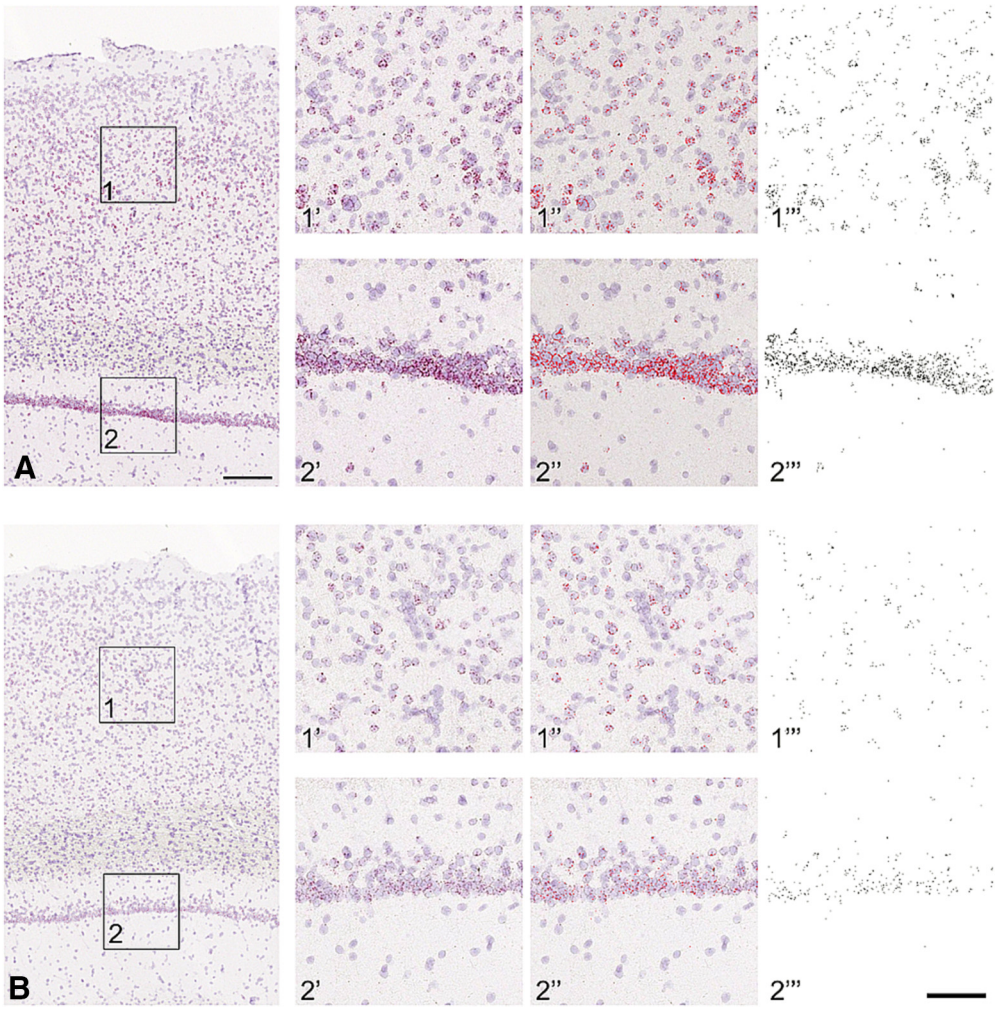

Figure 3. Examples of transcript isolation and thresholding in A1. ***A***, Young tissue. ***B***, Aged tissue. Boxes represent locations of panels centered on L4 (1) and CA2 hippocampus (2). ***A1′***, ***A2′***, ***B1′***, ***B2′***, Raw images from ***A*** and ***B***. ***A1″***, ***A2″***, ***B1″***, ***B2″***, Images after color thresholding. ***A1‴***, ***A2‴***, ***B1‴***, ***B2‴***, Images after binary thresholding and watershed separation. Transcript counts derived from particle counts by cortical layer. For details, see Materials and Methods. Scale bars: ***A***, ***B***, 250 um; ***A1′–B2‴***, 100 um.

tissue sections spaced 126 µm apart. Counts from the four hemispheres were averaged and treated as a single estimate for each case. As for Set 1, within-subject averaging was done to reduce measurement error due to random variability in staining between tissue sections from the same brain. Cell counts and SDs from the mean were tabulated and charted for reference to cell plots. Statistical comparisons of cell counts between hemispheres, layers, and marker combinations were not considered important experimental objectives of this study.

ChAT and AChE laminar profiles. Images and laminar profile plots of ChAT/NeuN IF and AChE histochemistry show typical expression of markers associated with cholinergic input to A1 in young-adult rats (Fig. 4*A–D*). Laminar profile plots of each marker were derived in Image J (Fiji). RGB images were converted to grayscale; then the profile plot function was used to measure relative grayscale density (0–255) from a line (~1600 × 250 pixels) extending from L1 to white matter and spanning the width of each image. No further analysis of these density patterns was done.

Receptor autoradiography. Groups of young (4–6 months, $N = 4$) and aged (28–33 months, $N = 4$) male FBN rats were decapitated and brains quickly removed, washed briefly with PBS slush, frozen in dry ice, and stored in −80°C. Frozen coronal sections (16-µm-thick) through A1 (bregma −6.04 mm to −4.80 mm) (Paxinos and Watson, 1998) were made using a cyrostat (Leica Microsystems, model CM1850), collected on slides and stored at −20°C for <48 h. Procedures for [^{3}H]epibatidine binding and image analysis were described in detail by Sottile et al. (2017a). Briefly, tissue sections were fixed in 4% PFA (Sigma Millipore) for 10 min at room temperature, prewashed with 50 mM Tris-HCl buffer containing 120 mM NaCl, 5 mM KCl, 2.5 mM $CaCl_2$, and 1 mM $MgCl_2$, pH 7.4, at room temperature by quick dips. After blotting residue of prewash buffer, sections were incubated at room temperature for 60 min in the same buffer above with 0, 0.1, 0.25, 0.5, 0.75, 1, and 1.5 nM of [^{3}H]epibatidine (PerkinElmer; specific activity = 62.2 Ci/mmol −1). Nonspecific binding was determined by incubating adjacent sections with 300 µM (–)-nicotine (Sigma Millipore) in the presence of increasing concentrations of [^{3}H]epibatidine. Incubation was stopped by washing slides twice with ice-cold buffer for 5 min each, followed by dipping them quickly in ice-cold dH_2O. Slides were air-dried overnight. Dried slides were opposed to [^{3}H]-hypersensitive phosphor screens (PerkinElmer) for 2 d at room temperature. Phosphor screens were scanned using a Cyclone Storage Phosphor System (PerkinElmer). The L2–L6 of A1 was outlined and analyzed using OptiQuant Image Analysis software (Canberra Packard-PerkinElmer), which provided tools for grayscale quantification in digital light units. Digital light units were then converted to nCi/mg protein using a standard curve generated from coexposed [3H]-embedded plastic standards (American Radiolabeled Chemicals) and further converted to fmol/mg protein. Values from the left and right A1 were combined.

Cortical slice electrophysiology. A1 nAChR dose–response studies used groups of young (4–6 months, $N = 8$) and aged (28–33 months, $N = 9$) male FBN rats. Rats were anesthetized with isoflurane (3%), and cardiac perfusion was performed using ice-cold sucrose aCSF (in mM as follows: 2.5 KCl, 5 $MgCl_2$, 1.23 NaH_2PO_4, 0.5 $CaCl_2$, 250 sucrose, 26

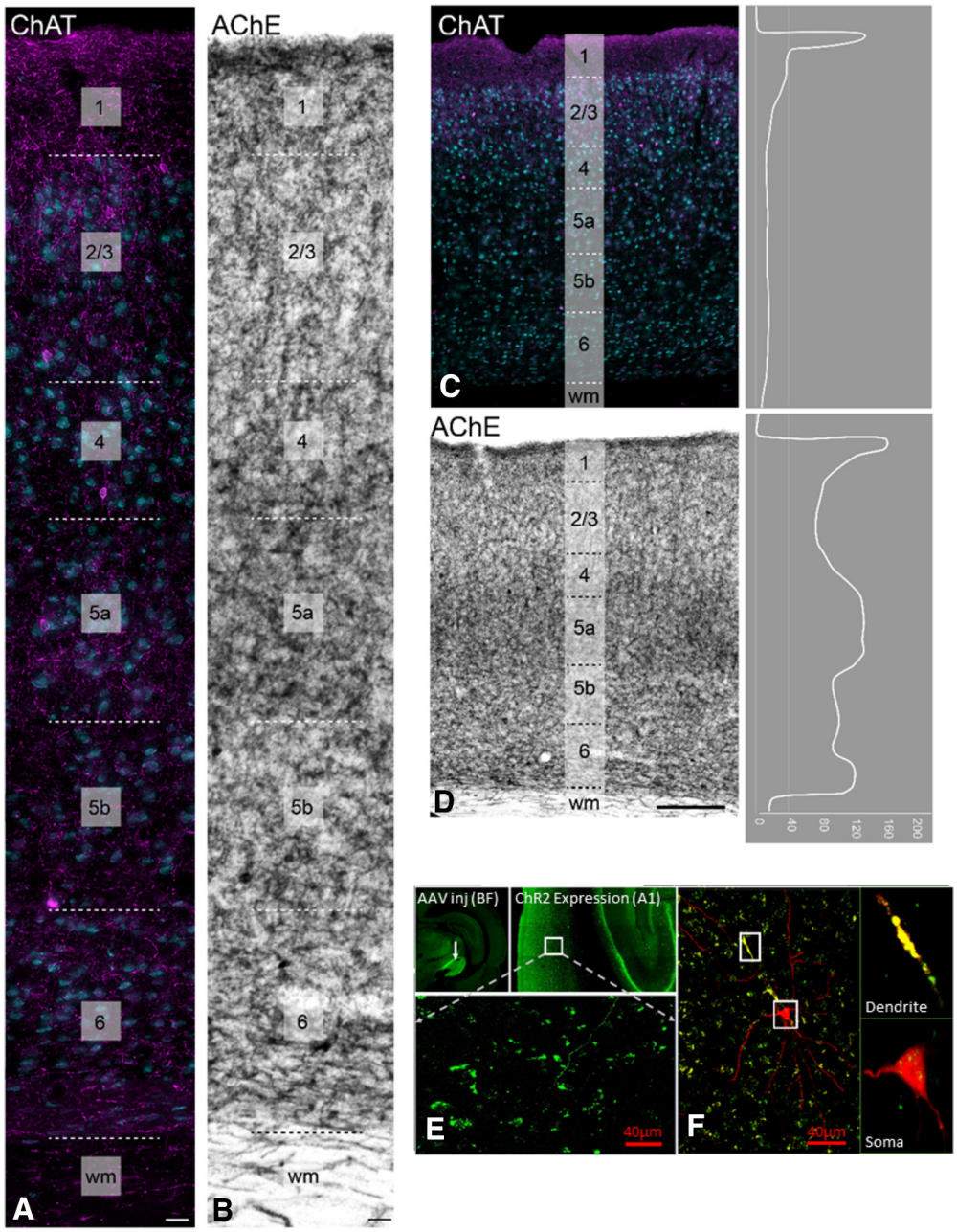

Figure 4. BF cholinergic inputs to A1. ***A***, ***C***, ChAT (magenta) and NeuN (blue) IF in A1. ***B***, ***D***, AChE histochemistry. ***C***, ***D***, Grayscale density profiles for ChAT and AChE across layers. ***E***, AAV (pAAV-Ef1a-DIO-hChR2(H134R)-EYFP-WPRE-pA) injection in BF (arrow) of a *ChAT-Cre* Long-Evans rat(*LE-Tg(Chat-Cre)5.1Deis*) with ChAT IF (green) in A1. ***F***, Cholinergic inputs from BF (green) to an exemplar L5B pyramidal neuron (red) that was strongly depolarized by puffed ACh. Colocalization (yellow) of the BF inputs and L5B neuron was shown in both dendrites (***F***, top right) and soma (***F***, bottom right). Laminar boundaries indicated in transparent vertical bars. wm, White matter. Scale bars: ***A***, ***B***, 25 μm; ***C***, ***D***, 250 μm; ***E***, 40 μm.

$NaHCO_3$, and 10 glucose, pH 7.4) saturated with carbogen (95% O_2/5% CO_2) before decapitation. Isoflurane was maintained during the entire perfusion process. After perfusion and decapitation, brains were rapidly isolated and submerged in cold (1°C-2°C) aCSF, pH 7.4, and oxygen saturation was maintained by bubbling with carbogen (95% O_2/5% CO_2). aCSF composition was as follows (in mM): 125 NaCl, 3 KCl, 1 $MgCl_2$, 1.23 NaH_2PO_4, 2 $CaCl_2$, 26 $NaHCO_3$, and 10 glucose. Coronal slices of 250–300 μm through A1 were sectioned using a vibratome (Pelco), following the protocol described by Sottile et al. (2017a,b) and Richardson et al. (2013), and incubated for 15 min at 31°C. Slices were allowed to equilibrate at room temperature (20°C–22°C) for 60 min in carbogen-bubbled aCSF before recording. Slices were then transferred to an immersion recording chamber (2 ml), perfused at 2–3 ml/min with aCSF bubbled with carbogen at room temperature, and imaged using QImaging Rolera bolt on differential interference contrast microscope (BX50WI; Olympus Optical) under a 40× water-immersion objective.

Whole-cell recordings. Patch-clamp recordings were performed in whole-cell configuration using 3-6 MΩ fire-polished micropipettes pulled from borosilicate glass (1.1 mm ID, 1.7 mm OD; Garner Glass). The internal pipette solution contained the following (in mM): 140.0 potassium gluconate, 1 NaCl, 2 $MgCl_2$, 10 HEPES, 2 Mg-ATP, 0.3 Na-GTP, 6.88 KOH, Osm: 300 mOsms, pH 7.3 (adjusted with KOH). Pipettes were connected to Multi-clamp 700B Amplifier (Molecular Devices), and cells were recorded in voltage-clamp mode held at −65 mV in 10 kHz sampling rate. The patch pipette was positioned in A1 output layer L5 with Giga-ohm (>4GΩ) seal and intracellular recordings achieved with series resistances ranging from 10-25 MΩ. Whole-cell capacitance, input resistance, and series resistance were determined by application of a 5 mV square pulse. Exclusion criteria included the following: (1) a resting

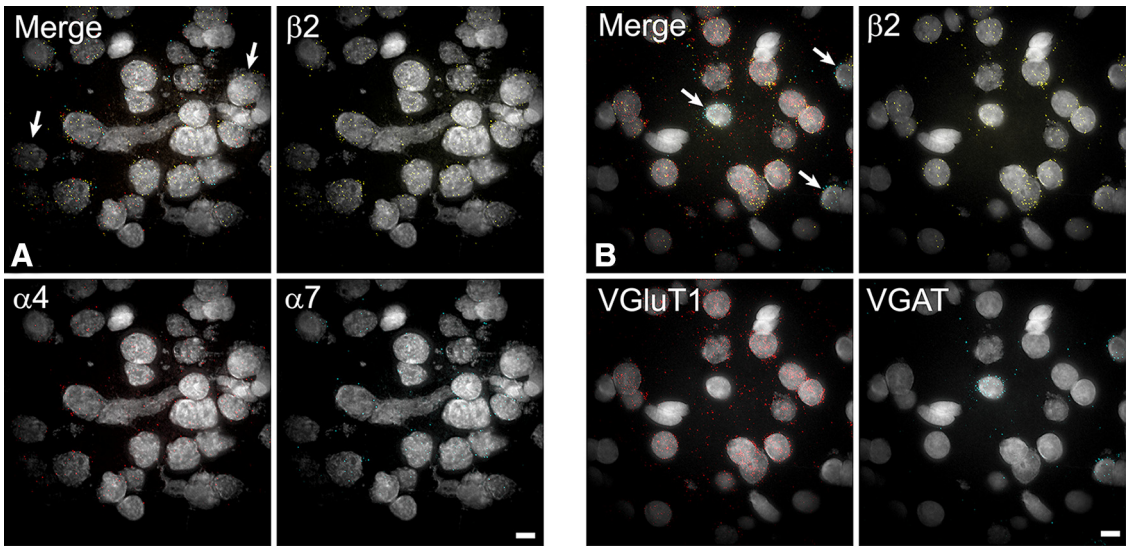

Figure 5. Examples of cellular phenotyping in A1 neurons. ***A***, Coexpression of β2 (yellow dots), α4 (red dots), and α7 (aqua dots) in L4 of A1. Arrows indicate cells containing β2 and α4, but not α7 transcripts. ***B***, Coexpression of β2 with *VGluT1* (red dots) and *VGAT* (aqua dots). β2 (yellow dots) is expressed in several glutamatergic (*VGluT1*$^+$) neurons, and 3 *VGAT*$^+$ neurons (arrows). Light gray represents DAPI. Scale bars, 10 μm.

membrane potential more depolarized than −60 mV, (2) series resistance >25 MΩ, (3) a resting input resistance <100 MΩ, and (4) data from less than for four doses of ACh. Generated TTL pulses, voltage commands, acquisition, and display of the recorded signals were achieved with Digidata 1440A (Molecular Devices) using the Clampex 10.7 program.

Stereotaxic injections and tracing. *ChAT-Cre* young-adult Long-Evans [4 months, *LE-Tg(Chat-Cre)5.1Deis*] rats were anesthetized using 1.4 ml/kg Ketamine (100mg/ml) and Xylazine (20mg/ml) mixture (3K:1× induction) and 0.5% isoflurane (maintenance). Animals were head-fixed in stereotaxic apparatus (Harvard Apparatus), and a midline incision was made to expose the skull. A craniotomy 1.5 mm was made to make a microinjection at AP −2.7, ML −4 and DV −7.3, corresponding to Substantia Innominata of Basal Forebrain. Approximately 150-200 nl pAAV-Ef1a-DIO-hChR2(H134R)-EYFP-WPRE (UNC Vector Core) was injected, and animals were allowed to recover and express the virus for a minimum of 3 weeks. Coronal slices (300 μm) of auditory cortex were produced as described above. Electrodes filled with internal solution containing Neurobiotin-350 (Vector Laboratories) were used to patch neurons in whole-cell configuration. Neurobiotin-350 was allowed to passively diffuse in patched cells for 20 min. After 20 min, the patch pipette was slowly detached to minimize damage to the cell. Slices were immediately fixed (4% PFA for 30 min.) followed by 3–5 washes in PBS to clear external Neurobiotin spilled while maintaining the positive pressure in the patch pipette. Slices were fixed overnight in 4% PFA, transferred onto plus-charged slides, and coverslipped with prolong gold until imaged. Images were acquired on a confocal LSM 800 Microscopic Imaging System (Carl Zeiss). 3D reconstruction of images was done using ZEN Blue 2.6.

Drug application. All experiments were done in the presence of atropine (20 μM) (Sigma Millipore), which was added to the aCSF bath solution. A patch pipette containing varying concentrations of ACh was positioned 30 μm from the patched cell under recording, and the drug was pressure ejected (5–7 psi) from a Picospritzer (General Valve). Based on pipette distance and inherent diffusion, the ACh concentration onto the surfaces of the recorded neurons was lower than the original pipette concentration. Based on findings from a previous *in vitro* drug application study (Uteshev et al., 2014), we calculated the cell surface concentration of ACh adjusted for distance and puffing time. The calculated 10–12^{-1} reduction in pipette concentration at the recorded cell surface provided dose values of ACh concentration as 10, 50, 100, and 500 μM and 1 mM. These concentrations are supported by Clements (1996), who estimated that neurotransmitter concentrations in a single vesicle vary between 60 and 210 mM, while estimates of peak synaptic cleft concentrations are suggested to be as high as high as 1–5 mM. McCaman et al. (1977) found that a 20 ms pulse at 10 psi released ~10–20 pl of solution from an ACh filled pipette. This corresponds to 10–20 e^{-15} mol of ACh when using a 1 mM stock solution, a release thought to approximate physiologic concentration at the soma. Although estimates of pressure pipette applied neurotransmitter concentrations at the synapse of the cell being studied are challenging, we suggest that concentrations used here were within estimated physiological range.

Subunit-selective nAChR antagonists were tested to determine whether age-related differences in postsynaptic currents (PSCs) evoked at 100 μM could be explained by changes in heteromeric versus homomeric nAChR subunit makeup. The α4β2 selective antagonist dihydro-β-erythroidine (DHβE, 100 nM, Sigma Millipore) and α7-selective antagonist methyllycaconitine (MLA, 100 nM, Sigma Millipore) were separately added to the aCSF bath in the presence of atropine (20 μM, Sigma Millipore). ACh postsynaptic responses in the presence of DhβE or MLA were tested repeatedly for 5 min to assure DhβE or MLA fully circulated in the bath. Percentage of inhibition was calculated based on the peak ACh control evoked amplitudes for each recorded neuron.

Statistical and data analysis. Electrophysiological data were analyzed using Clampfit 10.7 (Molecular Devices). The signals obtained were filtered using lowpass Gaussian filter (1 kHz), averaged, and the peak amplitude was determined during the 5 s interval after drug application. Statistical analysis was performed using SPSS 26 (IBM), and all statistical tests corresponding to the data are noted in the figure legends. Student's *t* tests were used for individual sample comparison and a one-way/two-way ANOVA with a Bonferroni *post hoc* correction was used for multiple comparisons. Data were tested for the homogeneity of variance, and the *p* values were corrected based on Levene's statistical significance. GraphPad Prism 7 was used for the analysis of autoradiography data to obtain B_{max} and dissociation constant (K_d). Data and statistical tests for ISH, cellular phenotyping, and whole-cell electrophysiology are described above in the related sections and in the figure legends. All comparisons with p value <0.05 were considered significant.

Results

A1 neurons and their dendritic terminals receive putative cholinergic inputs from BF (Fig. 4) (Nelson and Mooney, 2016). ChAT IF revealed dense ChAT$^+$ axons and terminals in all layers of A1 (Fig. 4*A*,*C*). AChE histochemistry showed reactivity in all layers,

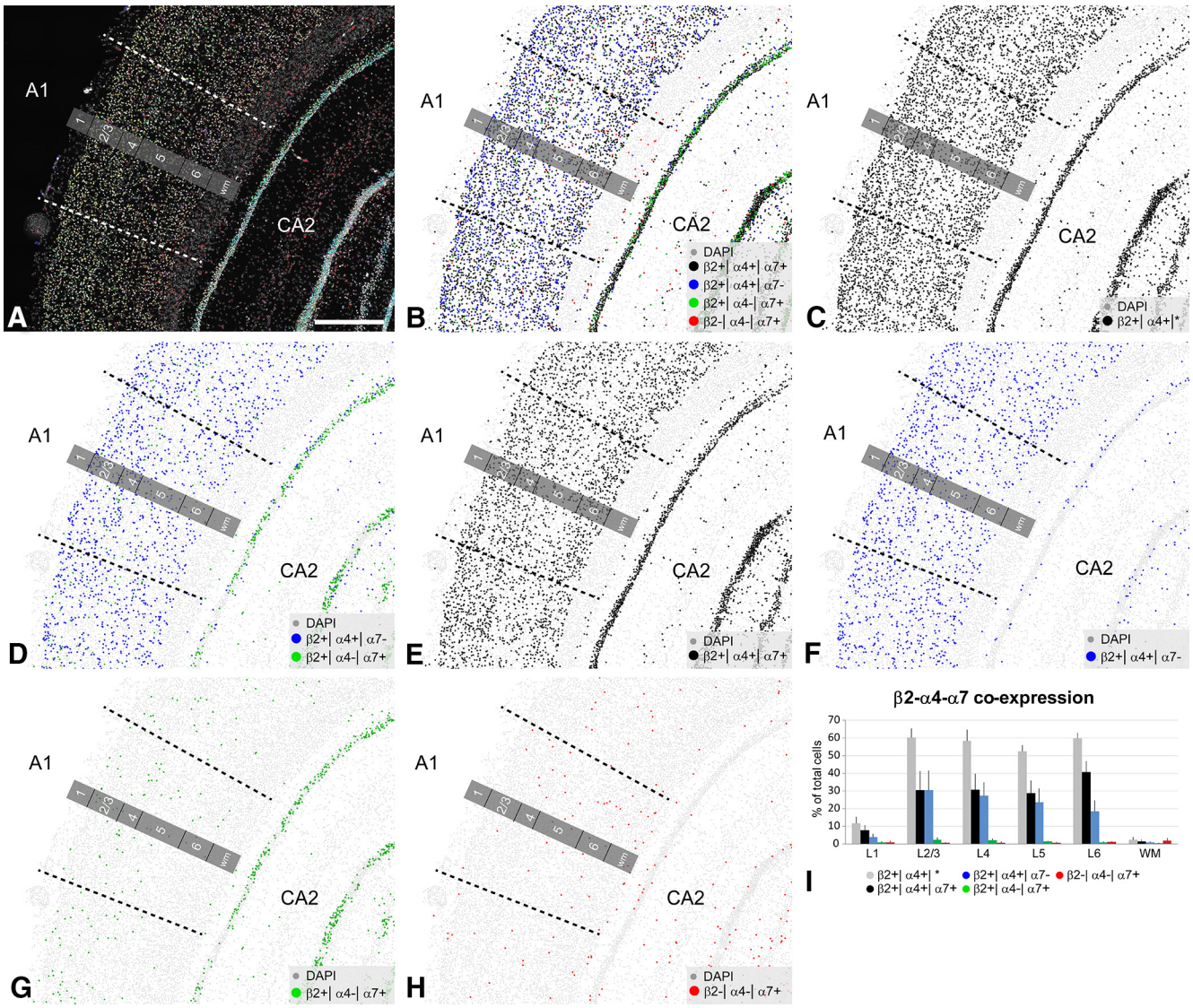

Figure 6. nAChR subunit coexpression in A1 cells. ***A***, Merged plot of all cells containing β2, α4, or α7 transcripts. ***B***, Plots of cells with subunit combinations shown in ***D–H***. ***C***, $\beta2^{+}\alpha4^{+}$* cells (black circles). *Any other transcript combination. ***D***, $\beta2^{+}\alpha4^{+}\alpha7^{-}$ (blue) and $\beta2^{+}\alpha4^{-}\alpha7^{+}$ (green) cells. ***E***, $\beta2^{+}\alpha4^{+}\alpha7$ cells (black). ***F***, $\beta2^{+}\alpha4^{+}\alpha7^{-}$ cells (blue). ***G***, $\beta2^{+}\alpha4^{-}\alpha7^{+}$ cells (green). ***H***, $\beta2^{-}\alpha4^{-}\alpha7^{+}$ cells (red). ***I***, Chart summarizing the proportion of total cells that expressed each subunit combination by A1 layer (mean of 4 animals + SD).

with peaks in L1a, L4-L5a, and L6b (Fig. 4*B*,*D*). An exemplar L5B pyramidal cell is seen to receive a rich cholinergic projection from EYFP-labeled BF neurons (Fig. 4*E*,*F*). This same neuron was strongly depolarized by ACh application (see Fig. 10). The presence of large numbers of nAChRs in A1 is confirmed by high levels of subunit message and receptor protein across the layers of A1, as detailed below.

nAChR subunit coexpression and distribution across young-adult A1 layers. Multiplex FISH assays were used to conduct cellular phenotyping as two separate sets. Set 1 combined riboprobes for β2, α4, and α7 to identify cells that coexpressed combinations of these nAChR subunits. Set 2 combined probes for a single nAChR subunit (β2, α4, or α7) with probes for glutamatergic (*VGluT1*, *VGluT2*) and GABAergic (*VGAT*) neurons. Figure 5 shows examples of cells labeled for these two combinations in A1. Figure 5*A* (top) show cells with $\beta2^{+}$, $\alpha4^{+}$, and $\alpha7^{+}$ transcripts coexpressed, of which two cells contain transcript for $\beta2^{+}$, $\alpha4^{+}$ only (arrow). Figure 5*B* (top) depicts an example of $\beta2^{+}$ (yellow dots) expression by several $VGluT1^{+}$ (glutamatergic) and two $VGAT^{+}$ (GABAergic) cells (arrows) in L3 of A1. These images were used to obtain counts of cells with specific transcript combinations (i.e., phenotypes).

The coexpression of nAChR subunits for combinations of β2, α4, and α7 is summarized in Figure 6, with a raw plot of all cells that expressed each combination overlaid on the original image (Fig. 6*A*). Figure 6*B* shows cells containing the four principal combinations, denoted by colored circles, with these combinations plotted separately in Figure 6*C*,*H*. Differential distributions of cell counts by combination and layer (Fig. 6*I*) indicate that ~60% of DAPI-labeled cells in A1 L2–L6 coexpressed β2 and α4. This 60% represented nearly equal proportions of cells (~30%) that coexpressed β2 and α4 with α7 ($\beta2^{+}$ $\alpha4^{+}\alpha7^{+}$) or β2 and α4 without α7 ($\beta2^{+}\alpha4^{+}\alpha7^{-}$) (Fig. 6*D–F*). Smaller subpopulations, widely distributed across layers, coexpressed β2 and α7 without α4 ($\beta2^{+}\alpha4^{-}\alpha7^{+}$) or α7 alone (Fig. 6*G*,*H*). Note the dense populations of cells containing α7 and β2, which is a heteromeric nAChR subtype known to exist in the CA2 region of hippocampus (Liu et al., 2012; Wu et al., 2016). Cell-sparse L1 contained cells that almost always coexpressed β2, α4, and α7 nAChR subunits. Overall, the results suggest that the α4β2 nAChR subtype predominates

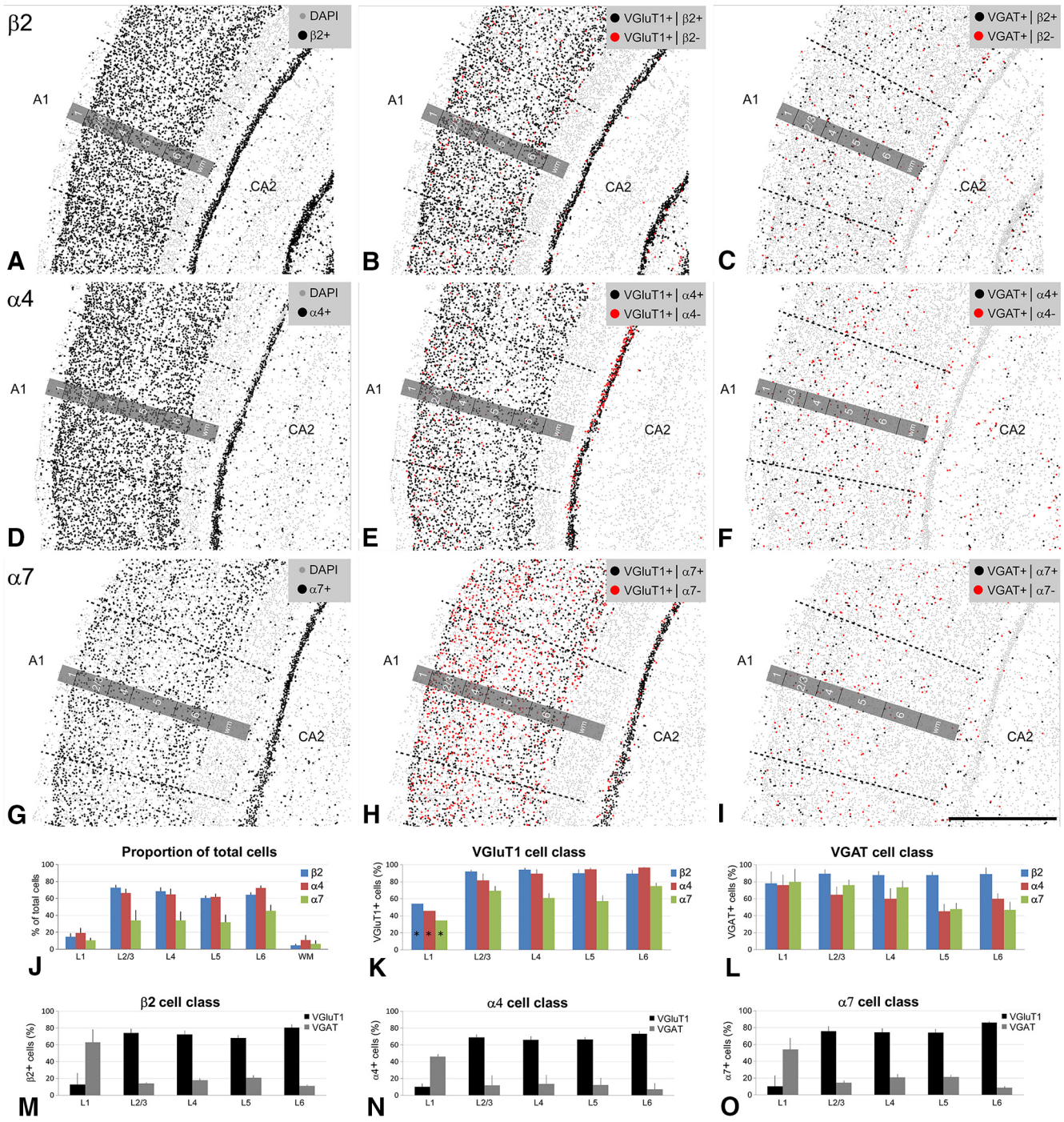

Figure 7. nAChR subunit coexpression by cell class in A1. ***A–I***, nAChR transcript expression plotted by cell class (*VGluT1* or *VGAT*), where each symbol represents one cell. Left column, Cells of any type containing β2, α4, or α7 transcripts. Middle column, *VGluT1*+ cells that did or did not coexpress β2, α4, or α7 transcripts. Right column, *VGAT*+ cells that did or did not coexpress β2, α4, or α7 transcripts. ***J–O***, Charts summarizing the proportions of cells that expressed each subunit, by cell class and layer. *SDs not calculated due to insufficient numbers of L1 *VGluT1*+ cells. Scale, 1 mm.

in A1, intermingled with other subtypes, including the α7 homomeric subtype and possibly the heteromeric α7β2 subtype. The significance of β2, α4, and α7 transcript coexpression in a substantial proportion of cells in A1 is not clear but could suggest that these cells express both α4β2 heteromeric and α7 homomeric nAChR subtypes.

nAChR subunit coexpression in excitatory and inhibitory young-adult A1 neurons. We next examined nAChR subunit coexpression patterns by major neurotransmitter cell class (Fig. 7). Plots of cells that express each subunit regardless of transmitter class are shown on the left (Fig. 7*A*,*D*,*G*) with nAChR subunit expression seen for putative glutamatergic cells (Fig. 7*B*,*E*,*H*) or putative GABAergic cells (Fig. 7*C*,*F*,*I*). β2 and α4 subunits were broadly expressed by the majority of neurons in all layers of A1 (Fig. 7*J–L*). The vast majority of *VGluT1*$^+$ neurons expressed β2 and α4 subunits (Fig. 7*K*), and ~65%-70% of β2$^+$ and α4$^+$ cells in L2–L6 were glutamatergic (Fig. 7*M*,*N*). α7 subunits were also found in the majority of *VGluT1*$^+$ neurons (Fig. 7*K*), although proportions were lower than β2 and α4, and ~70% of α7$^+$ neurons were glutamatergic (Fig. 7*O*).

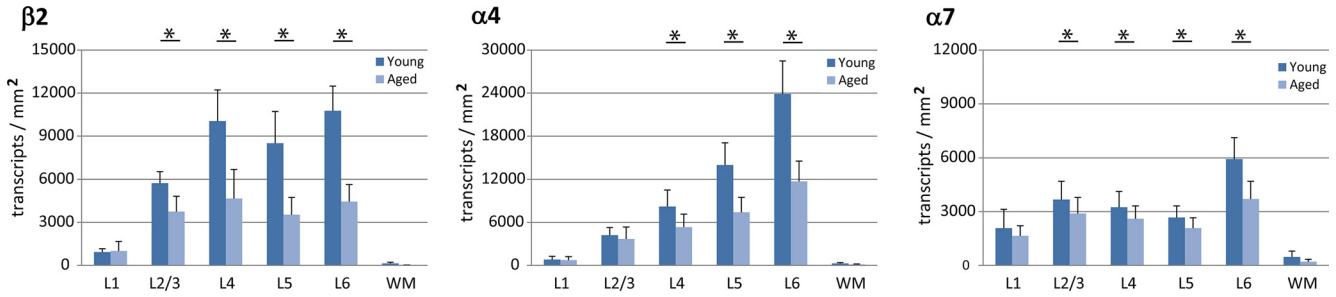

Figure 8. β2, α4, or α7 nAChR transcript density using ISH is depleted across A1 layers in aged animals. Normalized mean transcript density (mean ± SD) for β2 (left), α4 (middle), and α7 (right) in young (dark blue) and aged (light blue) A1 layers demonstrate significant downregulation of nAChR subunits with aging. *$p < 0.05$.

Table 3. β2, α4, or α7 nAChR transcript density across layers of FBN A1

		Young (mean ± SD)	Aged (mean ± SD)	% change	p	$t_{(df)}$
β2	L1	929 ± 228	999 ± 345	7.6 ± 29.7	0.77	$0.30_{(5)}$
	L2/L3	5739 ± 795	3749 ± 1070	−34.7 ± 19.6	0.043*	$2.70_{(5)}$
	L4	10037 ± 2189	4661 ± 1869	−53.5 ± 27.6	0.017*	$3.51_{(5)}$
	L5	8501 ± 2213	3532 ± 968	−58.4 ± 26.4	0.006*	$4.11_{(6)}$
	L6	10763 ± 1721	4448 ± 7711	−58.6 ± 16.3	0.001*	$6.66_{(5)}$
α4	L1	829 ± 439	679 ± 132	−18.1 ± 37.8	0.61	$0.57_{(5)}$
	L2/L3	4154 ± 771	3693 ± 777	−11.1 ± 19.7	0.47	$0.78_{(5)}$
	L4	8119 ± 1415	5338 ± 960	−34.2 ± 17.6	0.017*	$3.25_{(6)}$
	L5	14057 ± 2510	7407 ± 731	−47.3 ± 15.1	0.004*	$5.27_{(5)}$
	L6	23827 ± 3609	11722 ± 1386	−50.1 ± 14	0.002*	$6.28_{(5)}$
α7	L1	2198 ± 494	1639 ± 369	−25.4 ± 22.5	0.104	$1.87_{(7)}$
	L2/L3	3697 ± 293	2909 ± 186	−21.3 ± 7.2	0.002*	$4.65_{(7)}$
	L4	3172 ± 367	2597 ± 249	−18.1 ± 10.6	0.032*	$2.66_{(7)}$
	L5	2689 ± 144	2076 ± 366	−22.8 ± 10.7	0.01*	$3.47_{(7)}$
	L6	5831 ± 443	3701 ± 718	−36.5 ± 12.2	0.001*	$5.5_{(7)}$

* $p < 0.05$, statistically significant.

β2 subunits were expressed by over 80% of $VGAT^+$ neurons (Fig. 7*L*) in all layers. These proportions were somewhat lower for $\alpha4^+$ and $\alpha7^+$ nAChR subunits, especially in L5–L6. In L2–L6, 15%-20% of neurons containing β2, α4, or α7 transcripts were $VGAT^+$, contrasting with L1, where nearly all neurons were GABAergic and tend to coexpress β2, α4, and α7 (Figs. 6*I*, 7*L–O*) (Takesian et al., 2018). Cell numbers in L1 were very low, especially for the rare glutamatergic neurons; therefore, statistical comparisons may have low power (e.g., Fig. 7*K*; L1 $VGluT1^+$ cells).

Age-related changes in nAChR transcript density and distribution in A1. Because of auto-fluorescence artifacts associated with lipofuscin accumulation in aged tissue, chromogenic ISH was used instead of multiplex FISH for quantitative analyses to assess age-related changes in nAChR subunit transcript expression by cortical layer. Therefore, estimates of transcript abundance reflect global expression by all neuronal and glial cell classes in each layer. β2, α4, and α7 transcripts were detected in all cortical layers, but their densities varied by subunit, cortical layer, and age group. In young FBN rats, the density of nAChR α4 and β2 subunit transcripts tended to increase from superficial to deeper layers in A1 (Figs. 1, 8). This trend was most dramatic for the α4 subunit, which increased from a few hundred transcripts/mm^2 in L1 to nearly 24,000/mm^2 copies in L6. β2 subunit nAChRs transcripts were higher in L4–L6 than in L1–L3 (Fig. 8). The density of α7 transcripts was lower overall, and relatively evenly distributed across L2–L5, with a notable increase in L6.

Age-related declines in transcript density were observed for all three nAChR subunits examined (Fig. 8; Table 3). The declines were significant in most layers; and with some exceptions, relative levels generally maintained the laminar patterns observed in the younger cohort. For example, α4 nAChR density was reduced by ∼31% on average across layers in the older animals. In addition, the increase in density from L1–L6 observed in young animals was maintained in the older group, although the age-related decline became greater with cortical depth through L6 (Fig. 8; Table 3). For β2, the age-related decline averaged ∼39% overall but was decreased by ∼57% from L4–L6, effectively flattening the β2 density distribution from L2–L6. By comparison, α7 nAChR subunit expression was substantially lower in both age groups compared with α4 and β2. Unlike the near 50%–60% age-related decline seen for α4 and β2 nAChR subunit expression, α7 showed a relatively flat (<25%) decline across L1–L5, which peaked at 36% in L6 (Fig. 8; Table 3).

Aging and receptor binding at heteromeric nAChRs. To examine the presence of functional nAChRs across layers of A1, we undertook a series of autoradiographic saturation binding studies using the nAChR-selective compound [^{3}H]epibatidine, which has high affinity for all heteromeric nAChRs that contain a combination of α and β subunits (Xiao and Kellar, 2004). Similar to findings in somatosensory and visual cortex (Tizabi and Perry, 2000), sections through A1 showed higher density (B_{max}) of nAChRs in deeper A1 layers L4-L6 than in superficial L1–L3 (Fig. 9*A–F*). Consistent with the above findings for nAChR transcripts, [^{3}H]epibatidine binding showed a significant age-related loss in the number of heteromeric nAChRs (Fig. 9*F*; B_{max} mean ± SEM, layer, Y, O, $t_{(df)}$, p; L2/3, 85.52 ± 3.77, 60.97 ± 2.8, $t_{(14)} = 5.21$, $p = 0.0018$, L4, 124.1 ± 4.53, 95.14 ± 5.92, $t_{(14)} = 3.88$, $p = 0.00166$, L5, 100 ± 2.11, 83.42 ± 2.09, $t_{(14)} = 5.58$, $p = 0.00006$,

L6, 95.83 ± 2.31, 80.73 ± 1.53, $t_{(14)} = 5.44$, $p = 0.00008$). Specifically, the B_{max} was significantly decreased across A1 L2–L6 in aged animals. In addition, A1 L5 showed a significant decrease in the K_d, which suggested an increase in affinity for [^{3}H]epibatidine and may suggest possible nAChR subunit changes as well as a loss in the number of nAChRs (K_d, mean ± SEM, Y, O, 0.023 ± 0.0049, 0.0068 ± 0.0046, $t_{(14)}$ = 2.38, $p = 0.03$, t test) with nonsignificant decreases in K_d L4 and L6 ($n = 4$ animals/age group).

Impact of aging on layer 5 ACh-evoked nAChR responses. Increasing doses of ACh were puffed/applied onto voltage-clamped L5 pyramidal neurons in young and aged A1. All recordings from A1 *in vitro* slices used atropine (20 μM) to block muscarinic receptors. Increasing doses of ACh (10 μM to 1 mM) puffed onto patched young-adult pyramidal neurons resulted in increasing inward currents (Fig. 10*A*). Eighty percent of young A1 patched neurons (25 of 31) were responsive to puffed ACh, whereas 72% (26 of 36) of aged A1 pyramid neurons were responsive to puffed ACh. Bath application of TTX ($n = 3$) did not alter peak amplitude, confirming the postsynaptic nature of the responses. In contrast to the consistently increasing inward currents in young neurons, responses to ACh in aged neurons displayed saturation beginning at 100 μM, which plateaued between 100 and 500 μM ACh (Fig. 10*B*). Further application of ACh (1 mM) showed saturated/reduced responses (Fig. 10*B*). In agreement with the transcript and binding studies, patched L5 A1 neurons showed significant ($F_{(1,133)} = 9.44$, $p = 0.003$, two-way ANOVA) aged-related reductions in peak amplitude of ACh-evoked PSCs (Fig. 10*B*; peak amplitude mean ± SEM by dose: young = 0.01: 31.29 ± 6.84, 0.05: 44.8 ± 8.68, 0.1: 50.03 ± 9.86, 0.5: 57.71 ± 10.50, 1.0: 61.63 ± 10.92; and aged = 0.01: 24.3 ± 4.6, 0.05: 36.67 ± 9.03, 0.1: 36.38 ± 7.79, 0.5: 37.14 ± 6.71, 1.0: 29.13 ± 5.83). Signs of nAChR desensitization were observed at higher ACh dosages in recordings from A1 neurons in aged animals (dose 1 mM, $F_{(1,28)} = 6.89$, $p = 0.014$, one-way ANOVA; Fig. 10*B*). The significant age-related difference observed at 1 mM ACh suggests a possible impairment of cholinergic response at the time of high demand.

To selectively determine the relative contributions of heteromeric (α4β2) or homomeric (α7) nAChRs to PSCs evoked by puffed ACh (100 μM), subunit selective antagonists were added to the bath in a separate group of animals ($n = 3$ young, $n = 3$ old). The 100 μM ACh dosage (pipette concentration: 1 mM) was chosen based on the PSC plateau peak of the aged group. One neuron in the aged group ($n = 12$) showed no response to the α7 antagonist MLA, exceeding 2× SDs from the other neurons tested. It was considered an outlier and removed from the analysis. In the presence of atropine, this additional group of neurons showed an age-related reduction in peak amplitudes evoked by ACh (Fig. 10*C*, red bars; $f_{(1,41)} = 10.82$, $p = 0.002$, one-way ANOVA). The β2 selective antagonist, DHβE profoundly inhibited ACh-evoked PSCs from neurons in young rats (Fig. 10*C*, blue bar; $p < 0.0001$, Bonferroni *post hoc* test) and aged animals (Fig. 10*C*, blue bar; $p = 0.033$, Bonferroni *post hoc* test). Partial blockade of ACh-evoked currents was seen using the α7-selective antagonist MLA in L5 pyramidal neurons from young animals (Fig. 10*C*, green bar; ~18%, $p = 0.17$, Bonferroni *post hoc* test). A significant age-related increase in PSC blockade (Fig. 10*C*, green bar; ~44%, $p = 0.022$, Bonferroni *post hoc* test) was seen from L5 pyramidal neurons in response to MLA. When comparing peak amplitudes between DHβE blockade and MLA blockade, the

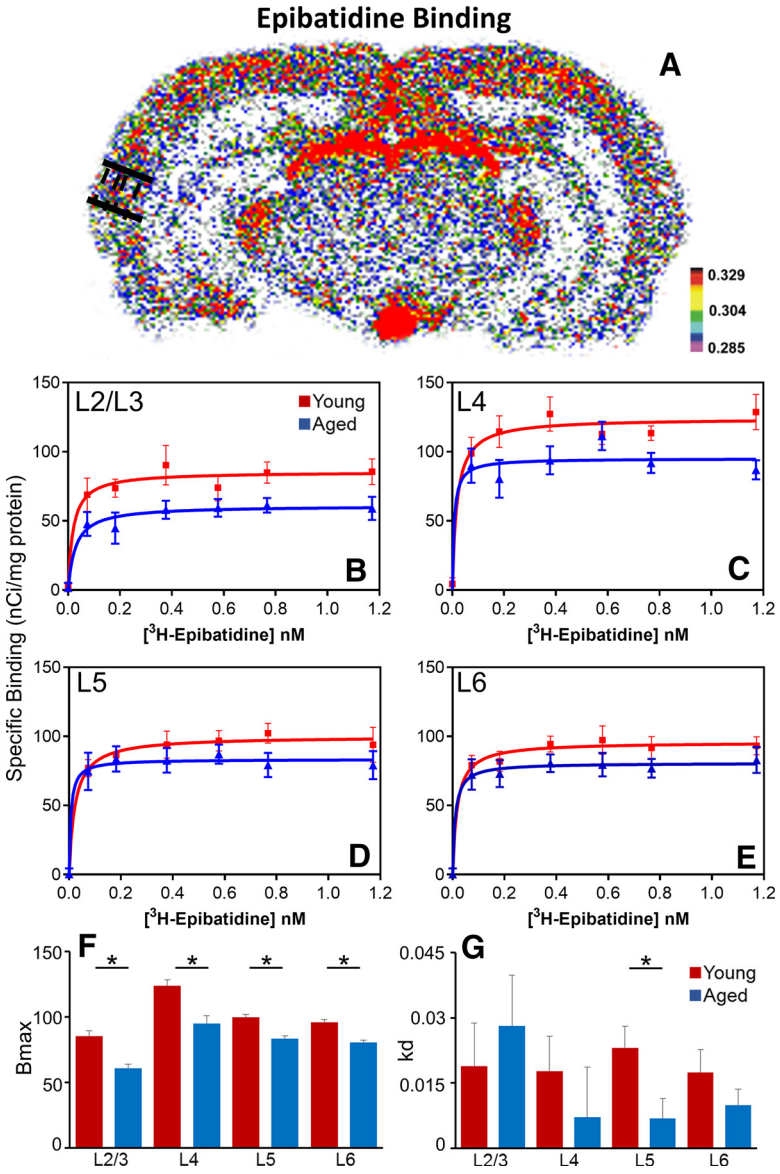

Figure 9. Significant loss of binding sites and increase in affinity with aging. ***A***, Exemplar autoradiograph (375 pM [^{3}H] epibatidine) of a cross-section through A1 shows high levels of nAChRs in the deeper A1 layers from a young FBN rat. Significant nAChR binding is also seen in the MGB, superficial layer of the superior colliculus (SC), and the interpeduncular nucleus (IPN). Nonspecific binding was measured in the presence of 300 μM nicotine. ***B–E***, Saturation binding curves show significant age-related loss of nAChRs density (B_{max}) across A1 layers plotted in histogram ***F***. There was a significant age-related increase in affinity (decrease in K_d) in L5 with no significant changes seen in L4 and L6 (***G***). *$p < 0.05$.

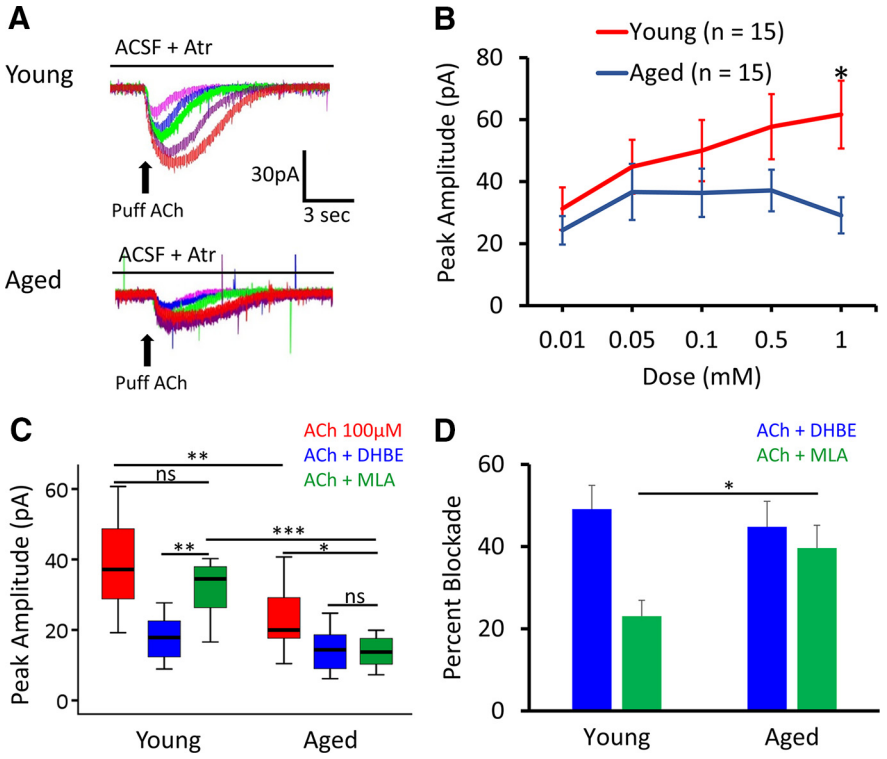

Figure 10. Age-related loss of differential nAChR mediates PSCs in L5 pyramidal neurons. Exemplar traces represent postsynaptic responses to local ACh application at 0.01 (pink), 0.05 (blue), 0.1 (green), 0.5 (purple), and 1.0 (red) mM from one young (***A***, top traces) and one aged (***A***, bottom traces) L5 pyramidal neuron, voltage-clamped at −70 mV. The mAChR blocker, atropine (Atr, 20 μM), was present in all experiments. ***B***, Dose–response curves compare local ACh application onto young (red, $n = 15$, 7 rats) and aged (blue, $n = 15$, 7 rats) L5 pyramidal neurons. A1 neurons showed a significant age-related (Two-way ANOVA, $F_{(1,133)} = 9.44$, $p = 0.003$, Two-way ANOVA, dose, age group) and single-point difference in peak amplitude at 1 μM (One-way ANOVA, dose 1.0, $F_{(1,28)} = 6.89$, $p = 0.014$). ***C***, Mean peak amplitude from L5 pyramid neurons in the presence of selective β2 (DHβE) and α7 (MLA) blockers in young and aged animals. Puffed ACh induced significantly smaller peak amplitude in neurons from aged rats than in neurons from the young rats ($t_{(40)} = 3.62$, $p = 0.001$, t test). DHβE dramatically inhibited the PSCs in neurons from young rat ($t_{(30)} = 6.09$, $p < 0.0001$, t test), with less of an effect in neurons from aged rats ($t_{(28)} = 2.3$, $p = 0.025$, t test). While MLA significantly inhibited PSCs in pyramidal neurons from aged animals ($t_{(28)} = 3.44$, $p = 0.002$, t test), a much smaller percentage blockade was seen in the reduction of PSCs from young animals ($t_{(32)} = 2.07$, $p = 0.046$, t test). ***D***, The percent change by selective nAChR blockade showed a significant age-related increase in relative MLA inhibition of the PSCs ($t_{(20)} = 2.14$, $p = 0.04$, t test). All the recordings were made in the presence of atropine. $^*p < 0.05$, $^{**}p < 0.01$, $^{***}p < 0.001$, ns = nonsignificant.

difference was significant in young animals (Fig. 10*C*; $p = 0.01$, Bonferroni *post hoc* test), but not significant (Fig. 10*C*; $p = 1$, Bonferroni *post hoc* test) in neurons recorded from aged animals. A significantly smaller (Fig. 10*C*; $f_{(1,21)} = 14.77$, $p = 0.001$, one-way ANOVA) residual peak excitability and a significant increase in percent blockade (Fig. 10*D*; $t_{(20)} = 2.14$, $p = 0.04$, t test) after α7 blockade with MLA were observed in aged animals. The findings of functional/pharmacological differences in the age-related changes of homomeric versus heteromeric nAChRs support the quantitative A1 L5 nAChR subunit expression results showing smaller age-related losses of α7 nAChR subunits relative to β2 subunits in aged rats.

Discussion

The A1 receives a major input from cholinergic neurons located in the BF subnuclei (Nelson and Mooney, 2016). When activated, BF projections may facilitate learning, selectively focus attention, and enhance cognition (Baxter et al., 1995; Kilgard and Merzenich, 1998; Hasselmo, 2006; Liang et al., 2008; Miller and Buschman, 2013; Maunsell, 2015). All of these functions show age-related changes (Cabeza et al., 2016). To maintain speech understanding temporally diminished by age-related peripheral changes and loss of central inhibition leading to a jittered acoustic message, older individuals upregulate use of these same cortical resources to help disambiguate speech (Ostroff et al., 2003; Pichora-Fuller et al., 2007; Wingfield and Tun, 2007; Caspary et al., 2008; Harris et al., 2010; Peelle et al., 2010; Fakhri et al., 2012; Leung et al., 2013; Peelle and Wingfield, 2016; Caspary and Llano, 2019).

The effectiveness of such compensatory mechanisms may be diminished in the elderly, in part due to reduced nAChR numbers in hippocampus and several forebrain areas (e.g., PFC, thalamus) (Picciotto and Zoli, 2002; Utkin, 2019). The present study examined the impact of aging on structural and functional features that contribute to nAChR-mediated cholinergic signaling in A1. The following are discussed below: (1) distinct differential nAChR transcript expression of the principal nAChR subunits across A1 layers; (2) age-related changes in nAChR transcript expression across A1 layers; (3) age-related changes in β2 containing nAChRs ([^{3}H]epibatidine binding) across A1 layers; and (4) age-related decreases in sensitivity to increasing doses of ACh applied to L5B pyramidal neurons in cortical slices.

Expression of β2, α4, α7 nAChR transcripts across A1 layers

The predominant nAChR subunits found in sensory neocortices are α4 and β2 subunits, which form heteromeric (e.g., 3α4 and 2β2) and homomeric nAChRs composed of five α7 subunits (Gotti et al., 2009). To date, no studies have quantified the laminar distributions of nAChR subunits in A1, but qualitative information is available in survey rat studies containing auditory cortex. In agreement with the present findings, which showed that the majority of glutamatergic and GABAergic neurons in L2–L6 express β2 and α4 subunit transcripts, two studies showed relatively high levels of β2 and α4 expression across L2–L6 in neocortex, including A1 (Wada et al., 1989; Son and Winzer-Serhan, 2008). Also matching our findings, images from these studies suggest increasing α4 expression from superficial L2 to deep L6 of A1. The present study also found that ~30% of L2–L5 neurons expressed all three nAChR subunits studied (β2, α4, α7), climbing to ~40% in L6 where α7 transcript density peaked, consistent with prior studies (Broide et al., 1995; Mugnaini et al., 2002; Son and Winzer-Serhan, 2008).

As observed in other mammalian neocortices, ~80% of A1 neurons are likely excitatory glutamatergic neurons, with ~20% being inhibitory GABAergic neurons. (DeFelipe et al., 2013; Ouellet and de Villers-Sidani, 2014). To our knowledge, phenotypic expression of nAChRs in inhibitory and excitatory A1

neurons has not been previously described. As might be expected from receptor binding and electrophysiological studies, a high percentage of excitatory glutamatergic and inhibitory GABAergic A1 neurons expressed the transcripts of all three subunits, consistent with actual numbers of these phenotypes across A1 layers. For example, L1 contains a relatively high proportion of GABAergic neurons that coexpress β2, α4 and α7, whereas the number of GABAergic cells expressing β2 nAChR transcripts exceeds the number expressing α4 nAChR transcripts in L2–L6. This leaves open the possibility that some number of α7 nAChR subunits not only form homomeric five α7 nAChRs, but may partner with β2 subunits forming the less common α7β2 heteromers, which has been reported in the hippocampus (Azam et al., 2003; Moretti et al., 2014; Wu et al., 2016). This is supported by the observation of $\beta2^{+}\alpha4^{-}\alpha7^{+}$ and $\beta2^{-}\alpha4^{-}\alpha7^{+}$ subpopulations in the present study.

[^{3}H]Epibatidine receptor binding for β2-containing heteromeric nAChR across A1 layers

Results from the present nAChR [3H]epibatidine saturation binding study are consistent with findings from four similar binding studies, which found highest levels for heteromeric nAChR binding concentrated around A1 L4, binding that is reduced by pruning thalamocortical inputs, while lower levels of nAChR binding were seen in deeper A1 layers (Clarke et al., 1985; Prusky et al., 1987; Sahin et al., 1992; Perry and Kellar, 1995; Han et al., 2003; Tribollet et al., 2004). Together, high levels of L4 binding support the previously described presynaptic location of heteromeric nAChRs on thalamocortical inputs, allowing BF ACh activation to increase glutamatergic excitation increasing ascending A1 information flow (Metherate, 2004; Gil and Metherate, 2019). The small but significant L5 increase in [3H] epibatidine binding affinity could reflect a change in the overall or cell-type-specific proportion of nAChR subunit subtypes remaining. Differential aging of subunits that may confer increased affinity over α4β2 nAChRs would include the α3β2, a subtype that showed slightly higher [3H]epibatidine binding affinity than α4β2 (Parker et al., 1998; Xiao and Kellar, 2004) and whose expression has been reported in whole cortex of young mice (Mao et al., 2008). If receptors composed of α3β2 or α4β2α5 subunits were less impacted by aging than α4 and/or β2, they could form higher affinity nAChR subtypes and underpin the observed increase in L5 nAChR affinity.

Discordance between message and protein across layer distribution of α4 and β2 nAChRs

While correlations between nAChR subunit (message) expression and its encoded receptor subunit protein might be expected, the relationship between mRNA and protein abundance is often not direct or predictive, as protein abundance is altered by various post-transcriptional regulatory processes and measurement methodologies (Ghazalpour et al., 2011; Vogel and Marcotte, 2012). In the present study, the numbers of cells in young-adult A1-expressing β2 and/or α4 transcripts were fairly stable across L2–L6, especially among excitatory neurons. Transcript density was highest in L4–L6 for β2 and increased steadily from L1–L6 for α4, roughly consistent with Wada et al. (1989) and single-cell sequencing in primary somatosensory cortex (Zeisel et al., 2015). Yet, these patterns differed from nAChR protein levels centered on L4. One potential explanation concerns differences in subcellular localization. nAChR mRNA transcripts are concentrated in the somatic cytoplasm, whereas receptor proteins may be localized to somata, dendrites, or axons positioned in different layers of the cortex or in projections from distant brain areas. [^{3}H]epibatidine receptor binding labeled somatic and dendritic distributions of assembled heteromeric nAChRs centered in and around L4 (Clarke et al., 1985; Perry and Kellar, 1995; Han et al., 2003; Tribollet et al., 2004), whereas the dendrites and axonal projections of neurons in L5−L6 are widely distributed across cortical layers and multiple brain regions (corticocortical, corticotectal, corticothalamic). This supposition is consistent with the findings of Sottile et al. (2017b), in which presynaptic nAChR activation by ACh enhanced glutamate release at corticothalamic terminals in the medial geniculate nucleus. Second, [^{3}H]epibatidine only binds/labels assembled heteromeric AChRs, not individual subunit proteins that have not been assembled into a receptor (Xiao and Kellar, 2004).

Impact of aging on nAChR subunit expression and nAChR binding across A1 layers

Significant age-related decreases in subunit expression were seen for the α4 (L4–L6), β2 (L2–L6), and α7 (L2–L6) nAChR subunits, with the age-related change proportionally smaller for the α7 putative homomeric nAChR subunit than the nAChR heteromeric-forming α4 and β2 subunits. The present age-related decreases seen for nAChR subunit transcripts in A1 were larger than those previously described for α4 and β2 subunits in whole neocortex, a study that also found no significant α7 nAChR subunit age-related message changes in neocortex (Ferrari et al., 1999). In agreement with the present findings, human and rat binding studies using ligands selective for β2-containing nAChR heteromers found significant age-related reductions in A1 (Marutle et al., 1998; Tribollet et al., 2004; Mitsis et al., 2009). Human temporal cortex showed a 19% (2.8% per decade) age-related decline of β2 containing nAChRs with smaller nonsignificant changes observed in whole rat neocortex (Picciotto and Zoli, 2002; Tribollet et al., 2004; Mitsis et al., 2009). Collectively, binding studies support significant reductions in heteromeric nAChRs with small age-related reductions or even an increase across life span for homomeric α7 containing subtypes (Utkin, 2019). Reviews of brain aging and nAChRs suggest that drugs targeting homomeric α7 nAChRs could be used to normalize cholinergic function with aging (Coughlin et al., 2018; Utkin, 2019).

Impact of aging on responses to ACh of A1 L5 pyramidal neurons

Finally, to functional evaluate the impact of aging on nAChRs, we examined responses of L5 pyramidal neurons to increasing doses (dose–response, 0.01-1 mM) of puffed ACh from A1 slices *in vitro*. As detailed in the Materials and Methods, we believe that concentrations of ACh applied here were within the estimated physiologic range (McCaman et al., 1977; Clements, 1996; Uteshev et al., 2014). There was an age-related decrease in nAChR responses at higher doses of ACh in pyramidal neurons from aged slices. This age-related reduction in the response of nAChRs to ACh could be due to the age-related loss of postsynaptic nAChRs causing full occupancy of ACh molecules on the remaining nAChRs. To understand the differential involvement of β2 and α7 nAChR subunits in cortical cholinergic signaling in young and aged rats, selective β2 and α7 antagonists DHβE and MLA were used. A significant age-related increase in the percentage of α7 nAChR-mediated PSCs was observed (18% in young vs 44% in aged) and is strongly suggestive of a selective age-related change in the subunit composition of nAChRs. α7 nAChRs have been described as having low affinity to ACh

and high desensitization rates (Fenster et al., 1997). Increased involvement of the α7 subunit in aged animals could explain the desensitization of the receptors seen at higher ACh concentrations.

In conclusion, the present findings map nAChR distributions in A1 by major cell class and show significant age-related changes in the abundance, physiology, and pharmacology of nAChRs, which are differentially distributed across layers and selectively impacted by aging. Differential pharmacological targeting of the nAChR constructs better maintained in aging may provide a first step strategy toward bolstering age-related declines in cognition and selective attention seen in the elderly. This approach could enhance the use of top-down resources needed to disambiguate speech in the elderly.

References

Askew CE, Lopez AJ, Wood MA, Metherate R (2019) Nicotine excites VIP interneurons to disinhibit pyramidal neurons in auditory cortex. Synapse 73:e22116.

Azam L, Winzer-Serhan U, Leslie FM (2003) Coexpression of alpha7 and beta2 nicotinic acetylcholine receptor subunit mRNAs within rat brain cholinergic neurons. Neuroscience 119:965–977.

Bakin JS, Weinberger NM (1996) Induction of a physiological memory in the cerebral cortex by stimulation of the nucleus basalis. Proc Natl Acad Sci USA 93:11219–11224.

Balaram P, Hackett TA, Polley DB (2019) Synergistic transcriptional changes in AMPA and GABAA receptor genes support compensatory plasticity following unilateral hearing loss. Neuroscience 407:108–119.

Ballinger EC, Ananth M, Talmage DA, Role LW (2016) Basal forebrain cholinergic circuits and signaling in cognition and cognitive decline. Neuron 91:1199–1218.

Bauer M, Kluge C, Bach D, Bradbury D, Heinze HJ, Dolan RJ, Driver J (2012) Cholinergic enhancement of visual attention and neural oscillations in the human brain. Curr Biol 22:397–402.

Baxter MG, Bucci DJ, Gorman LK, Wiley RG, Gallagher M (1995) Selective immunotoxic lesions of basal forebrain cholinergic cells: effects on learning and memory in rats. Behav Neurosci 109:714–722.

Bloem B, Poorthuis RB, Mansvelder HD (2014) Cholinergic modulation of the medial prefrontal cortex: the role of nicotinic receptors in attention and regulation of neuronal activity. Front Neural Circuits 8:17.

Broide RS, O'Connor LT, Smith MA, Smith JA, Leslie FM (1995) Developmental expression of alpha 7 neuronal nicotinic receptor messenger RNA in rat sensory cortex and thalamus. Neuroscience 67:83–94.

Cabeza R, Nyberg L, Park DC (2016) Cognitive neuroscience of aging: linking cognitive and cerebral aging. Oxford: Oxford UP.

Caspary D, Llano D (2019) Aging processes in the subcortical auditory system. In: The Oxford handbook of the auditory brainstem (Kandler K, ed), pp 639–680. Oxford: Oxford UP.

Caspary DM, Ling L, Turner JG, Hughes LF (2008) Inhibitory neurotransmission, plasticity and aging in the mammalian central auditory system. J Exp Biol 211:1781–1791.

Chaudhry FA, Reimer RJ, Bellocchio EE, Danbolt NC, Osen KK, Edwards RH, Storm-Mathisen J (1998) The vesicular GABA transporter, VGAT, localizes to synaptic vesicles in sets of glycinergic as well as GABAergic neurons. J Neurosci 18:9733–9750.

Clarke PB, Schwartz RD, Paul SM, Pert CB, Pert A (1985) Nicotinic binding in rat brain: autoradiographic comparison of [^{3}H]acetylcholine, [^{3}H]nicotine, and [^{125}I]-alpha-bungarotoxin. J Neurosci 5:1307–1315.

Clements JD (1996) Transmitter timecourse in the synaptic cleft: its role in central synaptic function. Trends Neurosci 19:163–171.

Colangelo C, Shichkova P, Keller D, Markram H, Ramaswamy S (2019) Cellular, synaptic and network effects of acetylcholine in the neocortex. Front Neural Circuits 13:24.

Coughlin J, Du Y, Crawford JL, Rubin LH, Behnam Azad B, Lesniak WG, Horti AG, Schretlen DJ, Sawa A, Pomper MG (2018) The availability of the alpha7 nicotinic acetylcholine receptor in recent-onset psychosis: a study using (18)F-ASEM PET. J Nucl Med 60:241–243.

DeFelipe J, López-Cruz PL, Benavides-Piccione R, Bielza C, Larrañaga P, Anderson S, Burkhalter A, Cauli B, Fairén A, Feldmeyer D, Fishell G, Fitzpatrick D, Freund TF, González-Burgos G, Hestrin S, Hill S, Hof PR, Huang J, Jones EG, Kawaguchi Y, et al. (2013) New insights into the classification and nomenclature of cortical GABAergic interneurons. Nat Rev Neurosci 14:202–216.

De Gois S, Schafer MK, Defamie N, Chen C, Ricci A, Weihe E, Varoqui H, Erickson JD (2005) Homeostatic scaling of vesicular glutamate and GABA transporter expression in rat neocortical circuits. J Neurosci 25:7121–7133.

Do JP, Xu M, Lee SH, Chang WC, Zhang S, Chung S, Yung TJ, Fan JL, Miyamichi K, Luo L, Dan Y (2016) Cell type-specific long-range connections of basal forebrain circuit. eLife 5:e13214.

Dumoulin A, Rostaing P, Bedet C, Levi S, Isambert MF, Henry JP, Triller A, Gasnier B (1999) Presence of the vesicular inhibitory amino acid transporter in GABAergic and glycinergic synaptic terminal boutons. J Cell Sci 112:811–823.

Evans DE, Drobes DJ (2009) Nicotine self-medication of cognitive-attentional processing. Addict Biol 14:32–42.

Everitt BJ, Robbins TW (1997) Central cholinergic systems and cognition. Annu Rev Psychol 48:649–684.

Fakhri M, Sikaroodi H, Maleki F, Ali Oghabian M, Ghanaati H (2012) Age-related frontal hyperactivation observed across different working memory tasks: an fMRI study. Behav Neurol 25:351–361.

Fenster CP, Rains MF, Noerager B, Quick MW, Lester RA (1997) Influence of subunit composition on desensitization of neuronal acetylcholine receptors at low concentrations of nicotine. J Neurosci 17:5747–5759.

Ferrari R, Pedrazzi P, Algeri S, Agnati LF, Zoli M (1999) Subunit and region-specific decreases in nicotinic acetylcholine receptor mRNA in the aged rat brain. Neurobiol Aging 20:37–46.

Fremeau RT Jr, Voglmaier S, Seal RP, Edwards RH (2004) VGLUTs define subsets of excitatory neurons and suggest novel roles for glutamate. Trends Neurosci 27:98–103.

Frisina DR, Frisina RD Jr, Snell KB, Burkard R, Walton JP, Ison JR (2001) Auditory temporal processing during aging. In: Functional neurobiology of aging, pp 565–579. Amsterdam: Elsevier.

Froemke RC, Merzenich MM, Schreiner CE (2007) A synaptic memory trace for cortical receptive field plasticity. Nature 450:425–429.

Geneser-Jensen FA, Blackstad TW (1971) Distribution of acetyl cholinesterase in the hippocampal region of the guinea pig: I. Entorhinal area, parasubiculum, and presubiculum. Z Zellforsch Mikrosk Anat 114:460–481.

Ghazalpour A, Bennett B, Petyuk VA, Orozco L, Hagopian R, Mungrue IN, Farber CR, Sinsheimer J, Kang HM, Furlotte N, Park CC, Wen PZ, Brewer H, Weitz K, Camp DG, Pan C, Yordanova R, Neuhaus I, Tilford C, Siemers N, et al. (2011) Comparative analysis of proteome and transcriptome variation in mouse. PLoS Genet 7:e1001393.

Gil SM, Metherate R (2019) Enhanced sensory-cognitive processing by activation of nicotinic acetylcholine receptors. Nicotine Tobacco Res 21:377–382.

Goard M, Dan Y (2009) Basal forebrain activation enhances cortical coding of natural scenes. Nat Neurosci 12:1444–1449.

Goodman L, Brunton L, Blumenthal D, Murri N, Hilal-Dandan RJ (2011) Appendix II: Design and optimization of dosage regimens: pharmacokinetic data. In: Goodman and Gilman's the pharmacological basis of therapeutics, Ed 12 (Brunton LL, Chabner BA, Knollman BC eds), pp 1787–1888. New York: McGraw-Hill.

Gordon-Salant S, Cole SS (2016) Effects of age and working memory capacity on speech recognition performance in noise among listeners with normal hearing. Ear Hear 37:593–602.

Gotti C, Clementi F, Fornari A, Gaimarri A, Guiducci S, Manfredi I, Moretti M, Pedrazzi P, Pucci L, Zoli M (2009) Structural and functional diversity of native brain neuronal nicotinic receptors. Biochem Pharmacol 78:703–711.

Grabinski TM, Kneynsberg A, Manfredsson FP, Kanaan NM (2015) A method for combining RNAscope in situ hybridization with immunohistochemistry in thick free-floating brain sections and primary neuronal cultures. PLoS One 10:e0120120.

Graziano A, Liu XB, Murray KD, Jones EG (2008) Vesicular glutamate transporters define two sets of glutamatergic afferents to the somatosensory thalamus and two thalamocortical projections in the mouse. J Comp Neurol 507:1258–1276.

Hackett TA (2018) Adenosine A1 receptor mRNA expression by neurons and glia in the auditory forebrain. Anat Rec (Hoboken) 301:1882–1905.

Hackett TA, Clause AR, Takahata T, Hackett NJ, Polley DB (2016) Differential maturation of vesicular glutamate and GABA transporter

expression in the mouse auditory forebrain during the first weeks of hearing. Brain Struct Funct 221:2619–2673.
Han ZY, Zoli M, Cardona A, Bourgeois JP, Changeux JP, Le NN (2003) Localization of [^{3}H]nicotine, [^{3}H]cytisine, [^{3}H]epibatidine, and [^{125}I] alpha-bungarotoxin binding sites in the brain of *Macaca mulatta*. J Comp Neurol 461:49–60.
Hangya B, Ranade SP, Lorenc M, Kepecs A (2015) Central cholinergic neurons are rapidly recruited by reinforcement feedback. Cell 162:1155–1168.
Harris KC, Eckert MA, Ahlstrom JB, Dubno JR (2010) Age-related differences in gap detection: effects of task difficulty and cognitive ability. Hear Res 264:21–29.
Hasselmo ME (2006) The role of acetylcholine in learning and memory. Curr Opin Neurobiol 16:710–715.
Ito T, Bishop DC, Oliver DL (2011) Expression of glutamate and inhibitory amino acid vesicular transporters in the rodent auditory brainstem. J Comp Neurol 519:316–340.
Itzkovitz S, van Oudenaarden A (2011) Validating transcripts with probes and imaging technology. Nat Methods 8:S12–S19.
Kaneko T, Fujiyama F, Hioki H (2002) Immunohistochemical localization of candidates for vesicular glutamate transporters in the rat brain. J Comp Neurol 444:39–62.
Kilgard MP, Merzenich MM (1998) Cortical map reorganization enabled by nucleus basalis activity. Science 279:1714–1718.
Kim JH, Jung AH, Jeong D, Choi I, Kim K, Shin S, Kim SJ, Lee SH (2016) Selectivity of neuromodulatory projections from the basal forebrain and locus ceruleus to primary sensory cortices. J Neurosci 36:5314–5327.
Kuchibhotla KV, Gill JV, Lindsay GW, Papadoyannis ES, Field RE, Sten TA, Miller KD, Froemke RC (2017) Parallel processing by cortical inhibition enables context-dependent behavior. Nat Neurosci 20:62–71.
Leaver AM, Renier L, Chevillet MA, Morgan S, Kim HJ, Rauschecker JP (2011) Dysregulation of limbic and auditory networks in tinnitus. Neuron 69:33–43.
Leung AW, He Y, Grady CL, Alain C (2013) Age differences in the neuroelectric adaptation to meaningful sounds. PLoS One 8:e68892.
Levin ED, McClernon FJ, Rezvani AH (2006) Nicotinic effects on cognitive function: behavioral characterization, pharmacological specification, and anatomic localization. Psychopharmacology (Berl) 184:523–539.
Liang K, Poytress BS, Weinberger NM, Metherate R (2008) Nicotinic modulation of tone-evoked responses in auditory cortex reflects the strength of prior auditory learning. Neurobiol Learn Mem 90:138–146.
Liu Q, Huang Y, Shen J, Steffensen S, Wu J (2012) Functional alpha7beta2 nicotinic acetylcholine receptors expressed in hippocampal interneurons exhibit high sensitivity to pathological level of amyloid beta peptides. BMC Neurosci 13:155.
Lysakowski A, Wainer BH, Bruce G, Hersh LB (1989) An atlas of the regional and laminar distribution of choline acetyltransferase immunoreactivity in rat cerebral cortex. Neuroscience 28:291–336.
Mao D, Perry DC, Yasuda RP, Wolfe BB, Kellar KJ (2008) The alpha4beta2alpha5 nicotinic cholinergic receptor in rat brain is resistant to up-regulation by nicotine in vivo. J Neurochem 104:446–456.
Marutle A, Warpman U, Bogdanovic N, Nordberg A (1998) Regional distribution of subtypes of nicotinic receptors in human brain and effect of aging studied by (+/-)-[^{3}H]epibatidine. Brain Res 801:143–149.
Maunsell JH (2015) Neuronal mechanisms of visual attention. Annu Rev Vis Sci 1:373–391.
McCaman RE, McKenna DG, Ono JK (1977) A pressure system for intracellular and extracellular ejections of picoliter volumes. Brain Res 136:141–147.
Metherate R (2004) Nicotinic acetylcholine receptors in sensory cortex. Learn Mem 11:50–59.
Metherate R (2011) Functional connectivity and cholinergic modulation in auditory cortex. Neurosci Biobehav Rev 35:2058–2063.
Metherate R, Cox CL, Ashe JH (1992) Cellular bases of neocortical activation: modulation of neural oscillations by the nucleus basalis and endogenous acetylcholine. J Neurosci 12:4701–4711.
Miller EK, Buschman TJ (2013) Cortical circuits for the control of attention. Curr Opin Neurobiol 23:216–222.
Mitsis EM, Cosgrove KP, Staley JK, Bois F, Frohlich EB, Tamagnan GD, Estok KM, Seibyl JP, van Dyck CH (2009) Age-related decline in nicotinic receptor availability with [(123)I]5-IA-85380 SPECT. Neurobiol Aging 30:1490–1497.
Moretti M, Zoli M, George AA, Lukas RJ, Pistillo F, Maskos U, Whiteaker P, Gotti C (2014) The novel alpha7beta2-nicotinic acetylcholine receptor subtype is expressed in mouse and human basal forebrain: biochemical and pharmacological characterization. Mol Pharmacol 86:306–317.
Mugnaini M, Tessari M, Tarter G, Merlo Pich E, Chiamulera C, Bunnemann B (2002) Upregulation of [^{3}H]methyllycaconitine binding sites following continuous infusion of nicotine, without changes of alpha7 or alpha6 subunit mRNA: an autoradiography and in situ hybridization study in rat brain. Eur J Neurosci 16:1633–1646.
Nelson A, Mooney R (2016) The basal forebrain and motor cortex provide convergent yet distinct movement-related inputs to the auditory cortex. Neuron 90:635–648.
Ostroff JM, McDonald KL, Schneider BA, Alain C (2003) Aging and the processing of sound duration in human auditory cortex. Hear Res 181:1–7.
Ouellet L, de Villers-Sidani E (2014) Trajectory of the main GABAergic interneuron populations from early development to old age in the rat primary auditory cortex. Front Neuroanat 8:40.
Parent M, Descarries L (2008) Acetylcholine innervation of the adult rat thalamus: distribution and ultrastructural features in dorsolateral geniculate, parafascicular, and reticular thalamic nuclei. J Comp Neurol 511:678–691.
Parker MJ, Beck A, Luetje CW (1998) Neuronal nicotinic receptor beta2 and beta4 subunits confer large differences in agonist binding affinity. Mol Pharmacol 54:1132–1139.
Paxinos W, Watson C (1998) The rat brain in stereotaxic coordinates. San Diego: Academic.
Peelle JE, Wingfield A (2016) The neural consequences of age-related hearing loss. Trends Neurosci 39:486–497.
Peelle JE, Troiani V, Wingfield A, Grossman M (2010) Neural processing during older adults' comprehension of spoken sentences: age differences in resource allocation and connectivity. Cereb Cortex 20:773–782.
Perry DC, Kellar KJ (1995) [^{3}H]Epibatidine labels nicotinic receptors in rat brain: an autoradiographic study. J Pharmacol Exp Ther 275:1030–1034.
Picciotto MR, Zoli M (2002) Nicotinic receptors in aging and dementia. J Neurobiol 53:641–655.
Pichora-Fuller MK, Schneider BA AC (2017) Older adults at the cocktail party. In: The auditory system at the cocktail party (Middlebrooks JC, Simon JZ, Popper AN, Fay RR, eds), pp 227–259. New York: Springer.
Pichora-Fuller MK, Schneider BA, Macdonald E, Pass HE, Brown S (2007) Temporal jitter disrupts speech intelligibility: a simulation of auditory aging. Hear Res 223:114–121.
Player AN, Shen LP, Kenny D, Antao VP, Kolberg JA (2001) Single-copy gene detection using branched DNA (bDNA) in situ hybridization. J Histochem Cytochem 49:603–612.
Prusky GT, Shaw C, Cynader MS (1987) Nicotine receptors are located on lateral geniculate nucleus terminals in cat visual cortex. Brain Res 412:131–138.
Radnikow G, Feldmeyer D (2018) Layer- and cell type-specific modulation of excitatory neuronal activity in the neocortex. Front Neuroanat 12:1.
Richardson BD, Ling LL, Uteshev VV, Caspary DM (2013) Reduced GABA (A) receptor-mediated tonic inhibition in aged rat auditory thalamus. J Neurosci 33:1218–1227a.
Roberts LE, Husain FT, Eggermont JJ (2013) Role of attention in the generation and modulation of tinnitus. Neurosci Biobehav Rev 37:1754–1773.
Sahin M, Bowen WD, Donoghue JP (1992) Location of nicotinic and muscarinic cholinergic and mu-opiate receptors in rat cerebral neocortex: evidence from thalamic and cortical lesions. Brain Res 579:135–147.
Sarter M, Givens B, Bruno JP (2001) The cognitive neuroscience of sustained attention: where top-down meets bottom-up. Brain Res Brain Res Rev 35:146–160.
Sarter M, Gehring WJ, Kozak R (2006) More attention must be paid: the neurobiology of attentional effort. Brain Res Rev 51:145–160.
Sarter M, Parikh V, Howe WM (2009) nAChR agonist-induced cognition enhancement: integration of cognitive and neuronal mechanisms. Biochem Pharmacol 78:658–667.
Schindelin J, Arganda-Carreras I, Frise E, Kaynig V, Longair M, Pietzsch T, Preibisch S, Rueden C, Saalfeld S, Schmid B, Tinevez JY, White DJ, Hartenstein V, Eliceiri K, Tomancak P, Cardona A (2012) Fiji: an open-source platform for biological-image analysis. Nat Methods 9:676–682.
Schofield BR, Hurley L (2018) Circuits for modulation of auditory function. In: The mammalian auditory pathways: synaptic organization and

microcircuits (Oliver DL, Cant NB, Fay RR, Popper AN, eds), pp 235–267. New York: Springer.

Son JH, Winzer-Serhan UH (2008) Expression of neuronal nicotinic acetylcholine receptor subunit mRNAs in rat hippocampal GABAergic interneurons. J Comp Neurol 511:286–299.

Sottile SY, Ling L, Cox BC, Caspary DM (2017a) Impact of aging on postsynaptic neuronal nicotinic neurotransmission in auditory thalamus. J Physiol 595:5375–5385.

Sottile SY, Hackett TA, Cai R, Ling L, Llano DA, Caspary DM (2017b) Presynaptic neuronal nicotinic receptors differentially shape select inputs to auditory thalamus and are negatively impacted by aging. J Neurosci 37:11377–11389.

Takesian AE, Bogart LJ, Lichtman JW, Hensch TK (2018) Inhibitory circuit gating of auditory critical-period plasticity. Nat Neurosci 21:218–227.

Terry AV Jr, Buccafusco JJ, Jackson WJ, Zagrodnik S, Evans-Martin FF, Decker MW (1996) Effects of stimulation or blockade of central nicotinic-cholinergic receptors on performance of a novel version of the rat stimulus discrimination task. Psychopharmacology (Berl) 123:172–181.

Tizabi Y, Perry DC (2000) Prenatal nicotine exposure is associated with an increase in [^{125}I]epibatidine binding in discrete cortical regions in rats. Pharmacol Biochem Behav 67:319–323.

Tribollet E, Bertrand D, Marguerat A, Raggenbass M (2004) Comparative distribution of nicotinic receptor subtypes during development, adulthood and aging: an autoradiographic study in the rat brain. Neuroscience 124:405–420.

Uteshev VV, Gusev AG, Sametsky EA (2014) Chapter 10. Network control mechanisms: cellular milieu. In: Neuronal networks in brain function, CNS disorders, and therapeutics (Faingold CL, Blumenfeld H, eds), pp 135–144. San Diego: Academic.

Utkin YN (2019) Aging affects nicotinic acetylcholine receptors in brain. Cent Nerv Syst Agents Med Chem 19:119–124.

Vogel C, Marcotte EM (2012) Insights into the regulation of protein abundance from proteomic and transcriptomic analyses. Nat Rev Genet 13:227–232.

Wada E, Wada K, Boulter J, Deneris E, Heinemann S, Patrick J, Swanson LW (1989) Distribution of alpha 2, alpha 3, alpha 4, and beta 2 neuronal nicotinic receptor subunit mRNAs in the central nervous system: a hybridization histochemical study in the rat. J Comp Neurol 284:314–335.

Wang F, Flanagan J, Su N, Wang LC, Bui S, Nielson A, Wu X, Vo HT, Ma XJ, Luo Y (2012) RNAscope: a novel in situ RNA analysis platform for formalin-fixed, paraffin-embedded tissues. J Mol Diagn 14:22–29.

West R, Alain C (2000) Age-related decline in inhibitory control contributes to the increased Stroop effect observed in older adults. Psychophysiology 37:179–189.

Wingfield A, Tun PA (2007) Cognitive supports and cognitive constraints on comprehension of spoken language. J Am Acad Audiol 18:548–558.

Wu J, Liu Q, Tang P, Mikkelsen JD, Shen J, Whiteaker P, Yakel JL (2016) Heteromeric alpha7beta2 nicotinic acetylcholine receptors in the brain. Trends Pharmacol Sci 37:562–574.

Xiao Y, Kellar KJ (2004) The comparative pharmacology and up-regulation of rat neuronal nicotinic receptor subtype binding sites stably expressed in transfected mammalian cells. J Pharmacol Exp Ther 310:98–107.

Zeisel A, Munoz-Manchado AB, Codeluppi S, Lonnerberg P, La Manno G, Jureus A, Marques S, Munguba H, He L, Betsholtz C, Rolny C, Castelo-Branco G, Hjerling-Leffler J, Linnarsson S (2015) Brain structure: cell types in the mouse cortex and hippocampus revealed by single-cell RNA-seq. Science 347:1138–1142.